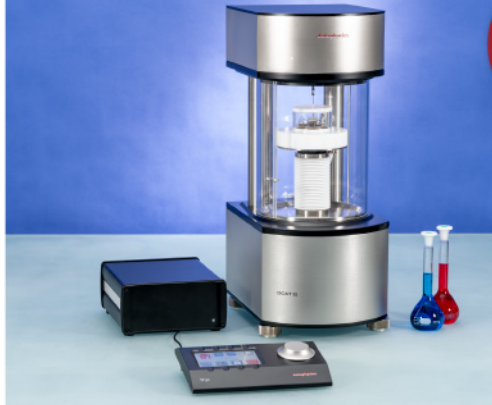




ASTM D5946
ASTM D7334
ASTM D7490
ISO 27448

optical contact angle measurements and drop contour analysis to determine surface energy as well as interfacial and surface tension

force tensiometry, dynamic contact angle measurements, and force of adhesion evaluation



ASTM D1331
ASTM D1417
ISO 1409

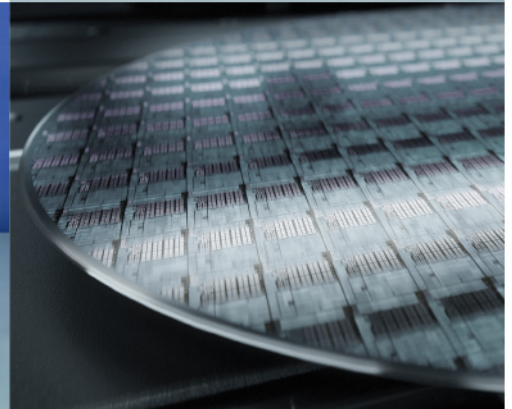


ISO/TR 13097

optical turbidity, stability and aging analysis of multi-phase dispersions



zeta potential measurements of fibres, powders, and plate-shaped solids



High-end, versatile laboratory measurement device portfolio for a comprehensive analysis of surfaces and interfaces

Learn more >

dataphysics
Understanding Interfaces

DataPhysics Instruments GmbH
Raiffeisenstraße 34 • 70794 Filderstadt, Germany
phone +49 (0)711 770556-0 • fax +49 (0)711 770556-99
sales@dataphysics-instruments.com
www.dataphysics-instruments.com

Programming Delayed Dissolution Into Sacrificial Bioinks For Dynamic Temporal Control of Architecture within 3D-Bioprinted Constructs


Bram G. Soliman, Alessia Longoni, Mian Wang, Wanlu Li, Paulina N. Bernal, Alessandro Cianciosi, Gabriella C.J. Lindberg, Jos Malda, Juergen Groll, Tomasz Jungst, Riccardo Levato, Jelena Rnjak-Kovacina, Tim B. F. Woodfield, Yu Shrike Zhang, and Khoon S. Lim*

Sacrificial printing allows introduction of architectural cues within engineered tissue constructs. This strategy adopts the use of a 3D-printed sacrificial ink that is embedded within a bulk hydrogel which is subsequently dissolved to leave open-channels. However, current conventional sacrificial inks do not recapitulate the dynamic nature of tissue development, such as the temporal presentation of architectural cues matching cellular requirements during different stages of maturation. To address this limitation, a new class of sacrificial inks is developed that exhibits tailorable and programmable delayed dissolution profiles (1–17 days), by exploiting the unique ability of the ruthenium complex and sodium persulfate initiating system to crosslink native tyrosine groups present in non-chemically modified gelatin. These novel sacrificial inks are also shown to be compatible with a range of biofabrication technologies, including extrusion-based printing, digital-light processing, and volumetric bioprinting. Further embedding these sacrificial templates within cell-laden bulk hydrogels displays precise control over the spatial and temporal introduction of architectural features into cell-laden hydrogel constructs. This approach demonstrates the unique capacity of delaying dissolution of sacrificial inks to modulate cell behavior, improving the deposition of mineralized matrix and capillary-like network formation in osteogenic and vasculogenic culture, respectively.

1. Introduction

Biomimicry of native tissue composition and architecture using cell-laden hydrogel constructs is widely recognized as a potential strategy for engineering functional tissue substitutes.^[1] Native tissue development (formation and maturation) and homeostasis are dictated by a series of dynamic processes, where cells are presented with physical and chemical stimuli in a spatiotemporally modulated manner.^[2–4] However, current tissue engineering and regenerative medicine strategies have not yet allowed recapitulation of these dynamic processes to fabricate large constructs of clinically relevant sizes. Given that oxygen and nutrient diffusion in large-scale hydrogels is restricted due to limitations in passive solute diffusion,^[5] the introduction of physical architectures, such as open and interconnected pores or perfusable channels, into cell-laden hydrogels has been shown to circumvent this problem.^[6,7] These physical architectures can furthermore be used to

B. G. Soliman, A. Longoni, G. C.J. Lindberg, T. B. F. Woodfield, K. S. Lim
Department of Orthopaedic Surgery & Musculoskeletal Medicine
Centre for Bioengineering & Nanomedicine
University of Otago
Christchurch 8011, New Zealand

 The ORCID identification number(s) for the author(s) of this article can be found under <https://doi.org/10.1002/adfm.202210521>.

© 2023 The Authors. Advanced Functional Materials published by Wiley-VCH GmbH. This is an open access article under the terms of the Creative Commons Attribution-NonCommercial-NoDerivs License, which permits use and distribution in any medium, provided the original work is properly cited, the use is non-commercial and no modifications or adaptations are made.

DOI: 10.1002/adfm.202210521

M. Wang, W. Li, Y. S. Zhang
Division of Engineering in Medicine
Department of Medicine
Brigham and Women's Hospital
Harvard Medical School
Boston, MA 02115, USA

P. N. Bernal, J. Malda, R. Levato
Department of Orthopaedics
University Medical Centre Utrecht
Utrecht University
3584 Utrecht, The Netherlands

A. Cianciosi, J. Groll, T. Jungst
Department for Functional Materials in Medicine and Dentistry at the Institute of Functional Materials and Biofabrication (IFB) and Bavarian Polymer Institute
University of Würzburg
97070 Würzburg, Germany

improve in vivo host tissue infiltration into hydrogels, e.g., in the case of blood vessel ingrowth into implanted constructs^[8] and bone ingrowth.^[9] Cells can also be subsequently seeded onto hydrogel scaffolds that contain these architectural elements, e.g. perfusing endothelial cells into open channels to generate endothelium-lined channels within the hydrogel, which has been demonstrated to facilitate improved integration between the scaffold and host tissue.^[10–12] Taken together, it is clear that introducing physical architectures into hydrogel-based engineered constructs can influence the overall tissue interaction and function, including formation, maturation and homeostasis.

Existing simple methods to impart physical architectures within hydrogels mainly revolve around micromoulding.^[13,14] Hydrogel-precursor solutions can for instance be cast around a needle and photo-cross-linked, after which the needle can be removed to yield an open channel.^[14] While micromoulding is attractive for the development of cell culture models to investigate cellular interactions at the interface of the open channel and the hydrogel, micromoulding principally lacks the spatial control to fabricate high-resolution architecturally relevant features. Over the past decades, the field of biofabrication has generated various technologies that enable spatial control over the fabrication of cell-free biomaterials and cell-laden hydrogel-based biomaterials, termed bioinks.^[6,12,15,16] Amongst the range of biofabrication technologies, extrusion-based printing (EBP),^[6,12,15,16] digital light processing (DLP)^[17] and more recently volumetric bioprinting (VBP)^[18] have been applied toward the generation of microchannels within large hydrogel-based constructs. EBP-enabled sacrificial printing in particular has been used due to its speed, high-precision and accessibility to 3D extrusion printer technology.^[19,20] The sacrificial printing process involves the extrusion of a sacrificial ink in a layer-by-layer fashion to prepare a sacrificial template. Subsequently, this sacrificial template is embedded within a bulk biomaterial, typically a hydrogel. At the onset of culture (i.e., within the first hours), the sacrificial template is finally dissolved or removed to leave open and perfusable features within the hydrogel construct. While current sacrificial inks allow spatial control over the physical structures, temporal control over the dissolution of sacrificial inks is lacking, with dissolution occurring rapidly and without temporal control at the onset of

culture at physiological temperature.^[6,12,15,16] As a result, current sacrificial printing methods fail to introduce architectural cues within bulk hydrogels in a temporally controlled manner, which is required to meet the dynamically varying demands of cells (e.g., oxygen and nutrient levels during tissue formation, maturation, and homeostasis). As an alternative to sacrificial printing, low degree of modification (DoM) methacryloyl-functionalized gelatin (Gel-MA) filaments have been reported to show cell-mediated enzymatic degradation after 12 days.^[21] Through direct filament stacking with non-degrading Gel-MA filaments, an open channel could be introduced. Filament stacking is however limited in its ability to introduce architectural cues when compared to sacrificial printing, and no programmability into the temporal dissolution of the low DoM Gel-MA filaments was demonstrated. Thus, there exists a need for a sacrificial ink that does not dissolve rapidly and without temporal control post-fabrication, but rather displays a varying or controllable dissolution rate to better mimic the dynamics of a developing tissue transitioning to a more mature, functional tissue.

Different materials have been used as sacrificial inks, including carbohydrate glass,^[6] Pluronics F-127,^[15,16] and gelatin,^[10,11] all of which have been successfully used to fabricate printable features of microscale resolution (<200 μm).^[6,16] More recently, poly(2-cyclopropyl-2-oxazoline) has been used to fabricate sacrificial templates through melt electrowriting, enabling the inclusion of small diameter (87 μm) channels within bulk hydrogels.^[22] In this study, we are particularly interested in gelatin, which has shear-thinning and thermosensitive viscoelastic properties that are adaptable to a range of printing technologies.^[23] In addition to its unique rheological profile, gelatin is water soluble and has abundant cell-adhesive sequences, which also makes it suitable as a cell-laden bioink – a feature that both carbohydrate glass and Pluronics F-127 do not possess.^[10–12] Furthermore, it has been previously shown that gelatin can be photo-cross-linked using the ruthenium-bipyridine complex (Ru) and sodium persulfate (SPS) co-photo-initiating system via the formation of di-tyrosine cross-links.^[24–27] Using chemically modified gelatin, the use of Ru/SPS as a co-initiating system has enabled the fabrication of hydrogels that exhibit a wide range of physico-chemical properties.^[28] Likewise, we hypothesize that by controlling and varying the degree of cross-linking in pristine gelatin, photo-cross-linked gelatin hydrogels that exhibit a wide range of physico-chemical properties, such as swelling and dissolution behavior, may be fabricated. The combination of gelatin with the Ru/SPS co-initiating system could consequently be an ideal candidate to design sacrificial bioink that does not dissolve at the onset of culture, but rather demonstrates delayed and programmable dissolution rates within relevant cell culture timeframes. To our knowledge, there are currently no sacrificial bioinks reported in the literature that are able to be used as cell-laden bioinks, as well as possess programmable dissolution features.

The aim of this study was to develop tailorable and programmable sacrificial printing inks to allow both spatial and temporal control of physical architectures within large hydrogel constructs. A further aim was to validate the effect of spatio-temporal introduction of microchannels within hydrogel constructs on cell behavior and functionality. First, the effect of gelatin, Ru and SPS concentrations on the resultant hydrogel

G. C.J. Lindberg
Phil and Penny Knight Campus for Accelerating Scientific Impact
Department of Bioengineering
University of Oregon
Eugene, OR 97403, USA

J. Malda, R. Levato
Department of Clinical Sciences
Faculty of Veterinary Medicine
Utrecht University
3584 Utrecht, The Netherlands

J. Rnjak-Kovacina
Graduate School of Biomedical Engineering
University of New South Wales
Sydney, NSW 2052, Australia

K. S. Lim
School of Medical Sciences
University of Sydney
Camperdown, NSW 2006, Australia
E-mail: khoon.lim@sydney.edu.au

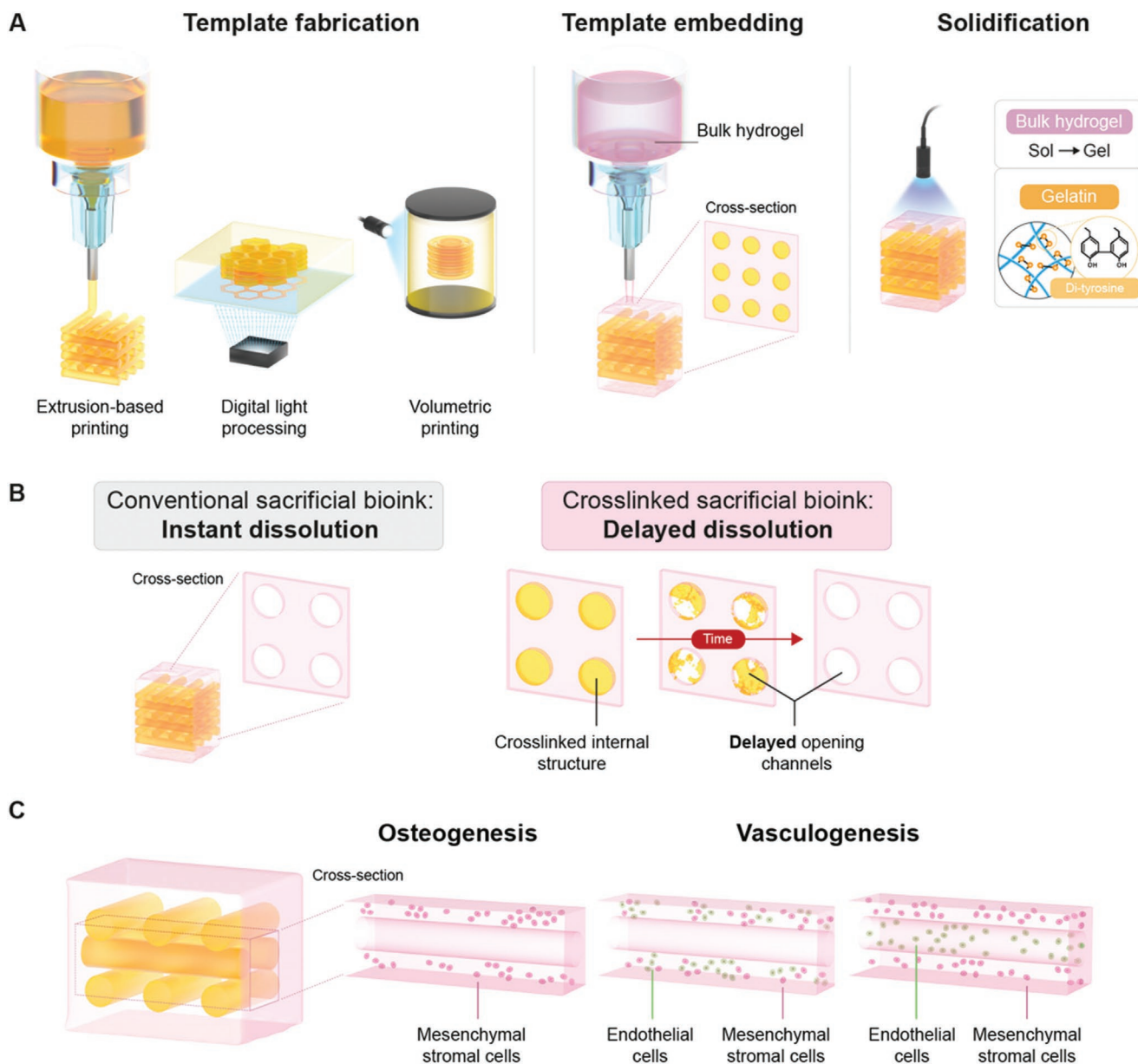


Figure 1. Schematic overview of delayed dissolution sacrificial printing platform for temporal introduction of microchannels. A) Fabrication of delayed dissolution sacrificial bioink consisting of pristine gelatin and the Ru/SPS photo-initiating system through extrusion-based printing (EBP), digital light processing (DLP), and volumetric bioprinting (VBP). After embedding of the sacrificial template in bulk hydrogel-precursor solution, the bulk hydrogel-precursor solution and gelatin sacrificial template is exposed to light to initiate photo-cross-linking. B) Where conventional sacrificial templates dissolve rapidly and without temporal control, leaving open channels, the photo-cross-linked sacrificial gelatin templates demonstrate delayed dissolution, only leaving open channels over time and in a controllable manner. C) The effect of the timing of sacrificial template dissolution on the behavior and functionality of encapsulated cells was assessed via osteogenesis and vasculogenesis tissue models.

dissolution rate is systematically investigated to establish the ability of this hydrogel platform for delayed dissolution. Then, the use of photo-crosslinkable gelatin as sacrificial inks is explored (Figure 1A) and applied across a range of biofabrication platforms, where the dissolution rate of sacrificial gelatin templates embedded within bulk hydrogels is investigated for the spatio-temporal introduction of physical architectures within these bulk hydrogels (Figure 1B). Finally, the effect of delaying sacrificial gelatin template dissolution on osteogenesis and neo-vascularization is evaluated in vitro (Figure 1C).

2. Results and Discussion

2.1. Tailoring Dissolution Profiles of Photo-Cross-Linked Gelatin Hydrogels for Use as Sacrificial Inks

Although photo-cross-linking of pristine gelatin hydrogels using the Ru/SPS co-initiating system has been previously reported,^[24] their dissolution rate has never been systematically examined. In this study, it was observed that in the presence of Ru/SPS, mechanically stable gelatin hydrogels could be

successfully fabricated within 1 min of visible light exposure (Figure S1A, Supporting Information). Notably, the substitution of the Ru/SPS photo-initiating system with other popular conventional type-I photo-initiators, such as Ig2959 and LAP, did not result in hydrogel formation, demonstrating that the ability to rapidly fabricate pristine gelatin hydrogels was unique to the use of type-II photo-initiators, such as Ru/SPS (Figure S1B, Supporting Information).

We hypothesized that the gelatin hydrogel dissolution rate could be tailored by controlling the cross-linking density, i.e., the amount of di-tyrosine bonds formed. Thus, we investigated the effect of hydrogel-precursor formulation on the resultant hydrogels' physico-chemical properties at various time points. Initially, the SPS concentration was varied (3–10 mM) in hydrogel-precursor solutions containing 10 wt.% gelatin and 0.1 mM Ru. The formation of di-tyrosine bonds within these hydrogels was verified through UV imaging, exploiting the autofluorescence of di-tyrosine bonds ($\lambda_{\text{ex}} = 315 \text{ nm}$).^[29,30] Under UV light, physically cross-linked gelatin hydrogel discs (10 wt.% gelatin gelled at low temperature, not photo-cross-linked) did not display any degree of fluorescence, indicating the lack of di-tyrosine bond formation (Figure S2A, Supporting Information). Meanwhile, photo-cross-linked gelatin hydrogels (10 wt.%, 0.1 mM Ru, 3–10 mM SPS) were visually fluorescent under UV light exposure, confirming the presence of di-tyrosine cross-links within these hydrogels (Figure S2B, Supporting Information). Increasing the SPS concentration in the gelatin precursor solutions did not result in any significant difference in the cross-linking efficiency with sol fraction values of $\approx 20\%$ obtained for all compositions (Table S1, Supporting Information), which are in the similar range to other previously reported gelatin-based hydrogel platforms.^[11,31] Instead, we observed an effect on the mass swelling ratio (28.9 ± 4.3 , 24.5 ± 1.9 , 25.0 ± 0.6 , and 20.9 ± 1.9 in formulations containing 3, 5, 7, and 10 mM SPS, respectively), where hydrogels prepared with higher SPS concentration had lower mass swelling ratio after 1 day (Table S1, Supporting Information). These results suggested that although increasing SPS concentration did not have any effect on the number of gelatin polymer chains retained within the hydrogel network (sol fraction), higher SPS concentration might instead contribute to the formation of more di-tyrosine cross-links within the network, hence the lower swelling observed. This observation was further supported through UV imaging of the photo-cross-linked gelatin hydrogels, where increasing the SPS concentration in the hydrogel-precursor solutions resulted in a concentration-dependent increase in fluorescence intensity of the fabricated gelatin discs (Figure S2C, Supporting Information). We believe that during light irradiation, the higher SPS concentration led to higher production rates of the free sulfate radical species, which subsequently resulted in higher cross-linking density.^[28] This trend was similarly observed when using the Ru/SPS system in a wide range of different macromers, including tyramine-functionalized poly(vinyl-alcohol) (PVA-Tyr),^[27] Gel-MA,^[32] gelatin-norbornene (Gel-NOR)^[7] and allylated gelatin (Gel-AGE).^[28]

During incubation at physiological temperature, a gradual increase in mass-loss (Figure 2A) and mass swelling ratio (Figure 2B) was observed. All evaluated hydrogel formulations

eventually reached a mass-loss of 100%, indicating the complete dissolution of the gelatin hydrogels. It was evident that the dissolution time of the gelatin hydrogels could be tailored from 2 to 15 days by adjusting the SPS concentration in the hydrogel-precursor solutions (Figure 2A). To gain a further understanding of how the concentrations of each of the components in the hydrogel-precursor solution (i.e., gelatin, Ru, and SPS) could affect dissolution time of the photo-cross-linked gelatin hydrogels, a systematic investigation into a wide array of hydrogel formulations was conducted. For this investigation, hydrogel discs were fabricated over a range of gelatin (5–10 wt.%), Ru (0.1–1 mM), and SPS (3–10 mM) concentrations (Figure 2C). A longer dissolution time was observed with increasing gelatin concentration. More specifically, increasing the gelatin concentration from 5 to 7.5 wt.% in formulations containing 0.5 mM Ru and 10 mM SPS resulted in an increase in dissolution time from 7.7 ± 1.5 to 10.3 ± 3.1 days, respectively. While keeping the Ru/SPS concentrations the same, further increasing the gelatin concentration (to 10 wt.%) led to a longer dissolution time of 13.7 ± 1.5 days. As increasing the gelatin concentration increased the number of tyrosine groups present, it was likely that increasing gelatin concentration resulted in an increase in the formation of di-tyrosine cross-links, thereby extending the dissolution time. In line with the results described earlier (Figure 2A,B), increasing the SPS concentration in the hydrogel-precursor formulation consistently resulted in an increased hydrogel dissolution time. However, it is interesting to note that the Ru component plays a minimal part in tailoring the dissolution time frame of gelatin hydrogels. For example, increasing the Ru concentration from 0.1 mM to 0.5 or 1 mM in formulations containing 5 wt.% gelatin and 10 mM SPS did not result in a significant change in dissolution time (7.3 ± 2.1 to 7.7 ± 1.5 and 7.7 ± 1.5 days, respectively). Overall, our results indicated that the dissolution time of photo-cross-linked gelatin hydrogels can only be modulated by the gelatin and SPS concentration, allowing dissolution to be tailored from 1.7 ± 0.6 to 15.0 ± 1.0 days. The nature of the photo-initiation mechanism utilized in this study explains the differences in the effect of Ru and SPS concentration on gelatin cross-linking and dissolution rate. During light irradiation, radical Ru^{2+} species undergo oxidation by reacting with SPS, forming Ru^{3+} species, sulfate radicals, and sulfate ions in the process.^[33,34] The Ru^{3+} species subsequently drive photo-oxidation of tyrosines into di-tyrosine cross-links.^[34] Due to the catalytic and recycling nature of Ru,^[33,34] a low Ru concentration was deemed sufficient to catalyze the photo-oxidative reaction in this study. The Ru^{3+} species subsequently drive photo-oxidation of tyrosines into di-tyrosine cross-links.^[34] Ruthenium is catalytic in nature as excited Ru species can be converted back to Ru^{2+} through subsequent subtraction reactions with water and oxygen, making Ru^{2+} available for further excitation.^[28] Due to the catalytic and recycling nature of Ru,^[33,34] a low Ru concentration was deemed sufficient to catalyze the photo-oxidative reaction in this study. However, SPS is depleted during the photo-oxidative reaction, forming a sulfate radical and sulfate ion after abstracting an electron from the excited Ru^{2+} species. Thus, increasing the SPS concentration likely allows for increased di-tyrosine bond formation as a result of the higher extent of photo-oxidative reaction that is possible. This explains why increasing the SPS

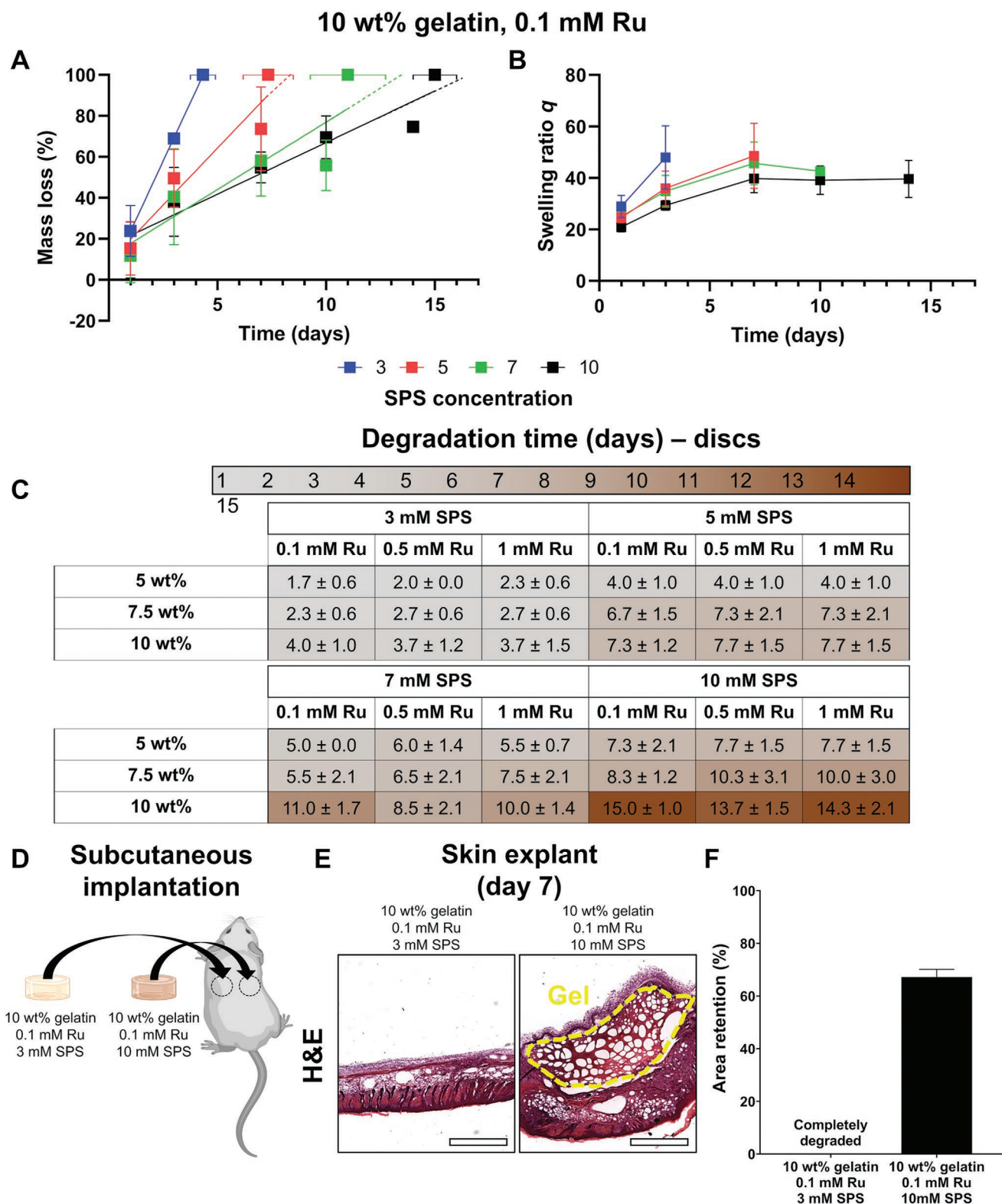


Figure 2. Tuneable dissolution profiles in photo-cross-linked gelatin discs. A,B) Mass loss and mass swelling profiles of 10 wt.% gelatin hydrogel discs (\varnothing 5 mm, 1 mm height), fabricated with 0.1 mM Ru and 3–10 mM SPS. C) Controlling degradation time of photo-cross-linked gelatin hydrogels by varying gelatin, Ru, and SPS concentration. D) Schematic overview of in vivo subcutaneous implantation mouse study. Two hydrogel formulations that dissolved completely within 4 days in vitro (10 wt.% gelatin, 0.1 mM Ru, and 3 mM SPS) and 15 days in vitro (10 wt.% gelatin, 0.1 mM Ru, 10 mM SPS) were selected. E) H&E staining of the hydrogel explants after 7 days. F) Quantitative area retention of hydrogel explants after 7 days. Scale bars = 1 mm. $N = 3$.

concentration (not Ru) within hydrogel-precursor formulations led to an increase in dissolution time of the resultant gelatin hydrogels in this study.

While it was clear that gelatin hydrogels displayed delayed dissolution *in vitro*, it was unclear whether gelatin hydrogels would display a similar capability for delayed dissolution *in vivo*. We thus selected two formulations that dissolved *in vitro* over a short period of time of 4 days (10 wt.% gelatin, 0.1 mM Ru, and 3 mM SPS) or over a longer period of 15 days (10 wt.% gelatin, 0.1 mM Ru, and 10 mM SPS) for *in vivo* characterization. Photo-cross-linked gelatin hydrogel discs of the selected formulations (2 mm in height, 5.5 mm in diameter) were subcutaneously implanted in Balb/c mice directly after hydrogel fabrication (Figure 2D). Skin explants taken after 7 days clearly showed intact skin at the subcutaneous implantation site where the hydrogel formulation that degraded *in vitro* within 4 days was no longer visible (Figure 2E). In contrast, the hydrogel formulation that degraded *in vitro* within 15 days was still clearly visible, retaining $672 \pm 2.9\%$ of the initial hydrogel area (Figure 2F). This proof-of-principle study clearly demonstrated that by controlling the number of di-tyrosine cross-links formed within gelatin hydrogels, the *in vivo* dissolution of these hydrogels can also be tailored in a similar fashion as the *in vitro* studies.

While it is encouraging that photo-cross-linked gelatin hydrogels displayed tailorable dissolution profiles within 1–15 days, their exact mode of degradation remains unclear. It is important to note that the photo-cross-linked gelatin hydrogels investigated in this study are incubated in phosphate buffered saline (PBS) that is not supplemented with any enzymes. Non-enzymatic catalyzed peptide hydrolysis is known to occur over a long time, with half-life of ≈ 500 – 600 years.^[35,36] Kirchmajer et al. previously reported that in the absence of matrix metalloproteases, gelatin hydrogels cross-linked using genipin did not degrade after 93 days.^[37] In another study, gelatin hydrogels cross-linked using lysine diisocyanate ethyl esters were only partially hydrolytically degraded ($\approx 30\%$ mass loss) over 280 days of incubation at physiological conditions.^[34] Given that the di-tyrosine cross-links that formed through the Ru/SPS photo-initiating system in this study are not known to be susceptible to hydrolysis,^[38,39] we believe that a different degradation mechanism exists for the relatively rapid (2 weeks) dissolution observed. Possibly, degradation of the gelatin hydrogels occurs through hydrolysis of the gelatin backbone as the hydrolysis rate of some amino acids at physiological conditions may occur at a slow, but relevant rate (e.g., 35 days for glycyglycines^[35]). Alternatively, excessive swelling may cause disruptions of hydrogen bonds present between gelatin chains and straining of the polymer network leading to breakage.^[40] In this case, the presence of di-tyrosine bonds could serve to delay the bulk degradation of the gelatin hydrogels during this process. While a full understanding of the exact mechanism of gelatin hydrogel dissolution was outside of the scope of the current paper, a clear correlation between the di-tyrosine cross-linking density and the observed hydrogel dissolution time existed. Future work could possibly further aid in providing a full understanding of the degradation mechanism through analysis of the hydrogel extract through techniques such as NMR, Fourier-transform infrared spectroscopy, and mass spectroscopy (see also Figure S3, Supporting Information).

2.2. Extrusion-Based Printing (EBP) of Delayed Dissolution Gelatin Inks as Sacrificial Templates

The ability to exploit the delayed dissolution of gelatin hydrogels to introduce physical architectures in the form of micro-channels within bulk hydrogels was investigated next. Pristine gelatin has previously only been used as a sacrificial ink without the addition of initiators or cross-linkers.^[12] In this paper, we demonstrated the ability to print sacrificial gelatin templates (5 to 10 wt.%) using inks composed of gelatin and the Ru/SPS co-initiators by exploiting the thermo-responsive rheological behavior and shear-thinning properties (Figure S4, Supporting Information). To enable EBP, collector temperature was maintained at 4 °C and printhead temperature was controlled at 22.0, 24.0, and 28.5 °C for 5, 7.5, and 10 wt.% gelatin, respectively. EBP of at least a six-layered (≈ 2.7 mm in height) lattice structure was successfully achieved, whereby increasing gelatin concentrations also resulted in improved print fidelity (Figure 3A). Scaled-up printing of constructs up to 10 layers (≈ 4.5 mm height) and 14 layers (≈ 6.3 mm height) was achieved using a 10 wt.% gelatin bioink, demonstrating minimal fiber sagging (Figure 3B). We were also able to demonstrate flexibility in designing the physical architecture of gelatin templates, where designs of constructs with angled filaments were successfully fabricated (Figure 3C). Moreover, the physical architectures can be varied within a single construct, where the fiber size/diameter (0.4, 0.6, and 0.8 mm diameter, Figure 3C) can vary not only in the x - y plane, but also in the z -plane (further characterization can be found in Figure S4, Supporting Information). These differences were achieved by altering the printhead movement speed and spindle speed of the printhead auger during the printing process. Physical architecture (*i.e.*, filament diameter, shape, and orientation) could have downstream effects on tissue formation by affecting factors such as media diffusion and nutrient supply.^[7,41] Thus, the high flexibility in gelatin template design demonstrated herein is an important feature of the developed sacrificial gelatin ink. Moreover, the wide range for the pristine gelatin inks successfully adopted for EBP (5–10 wt.%) was remarkable, considering that commonly used gelatin-based bioinks, such as Gel-MA are generally only able to be printed at higher polymer concentrations (>7 wt.%) as this high polymer content is required to maintain construct shape fidelity post-fabrication.^[31,42] As Gel-MA is a form of modified gelatin, it is known that the chemical modification process might reduce the physical interactions between gelatin chains through interference with hydrogen bonding,^[43] disrupting the native gelatin triple helix structures.^[44] Therefore, the wider printability of the pristine gelatin inks demonstrated in this study is most likely due to the formation of native physical cross-links between the gelatin chains.

Next, the ability to exploit the delayed dissolution of gelatin hydrogels to introduce physical architectures within bulk hydrogels was investigated (Figure 3D). Sacrificial gelatin inks containing 10 wt.% gelatin were selected due to the favorable printability of the sacrificial inks at this macromer concentration, ensuring good shape fidelity whilst allowing the largest possible range in dissolution time of photo-cross-linked sacrificial gelatin templates. For the remainder of this study, the following nomenclature in **Table 1** is used to refer to the relevant

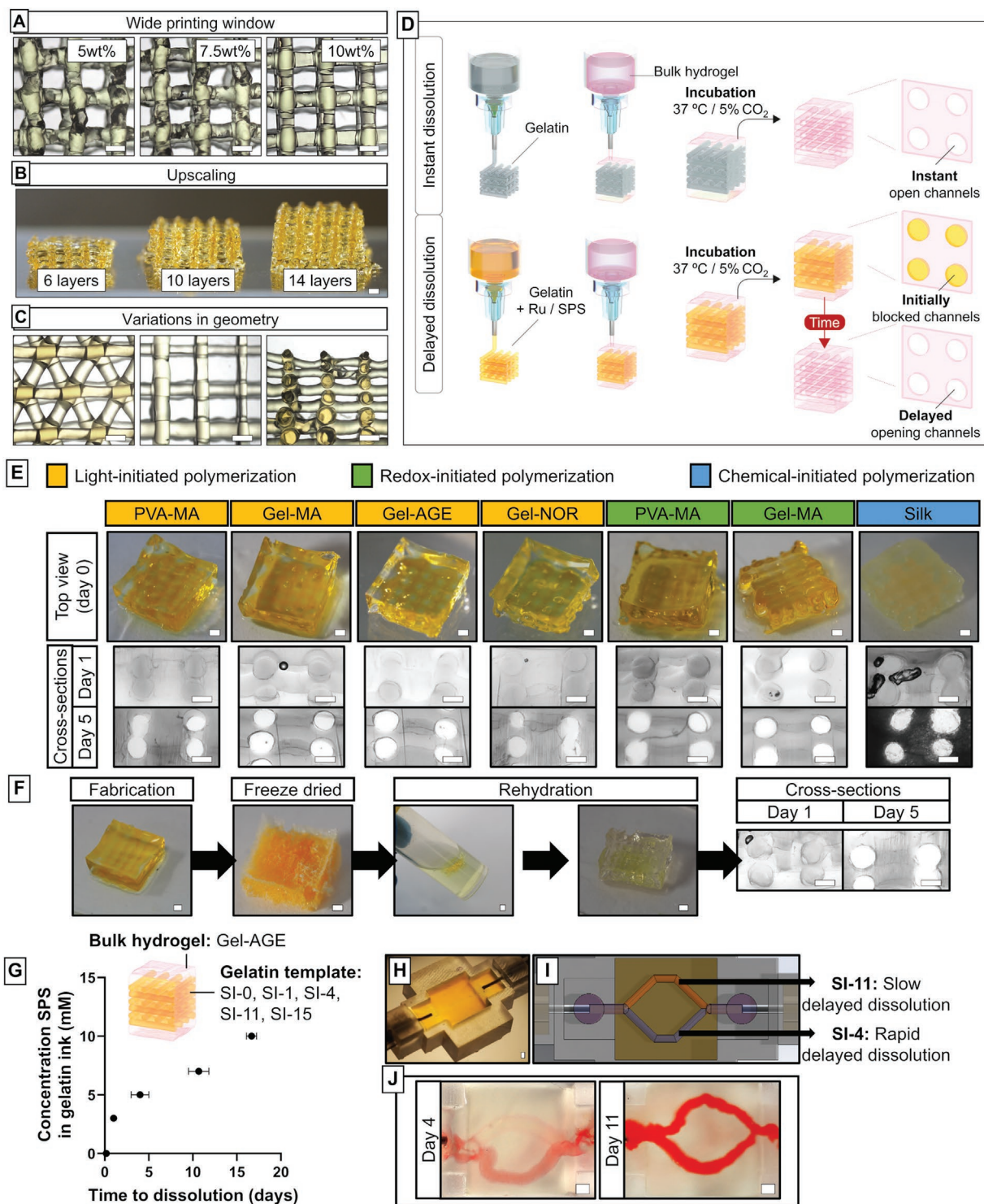


Figure 3. Extrusion-based printing (EBP) of delayed dissolution gelatin inks as sacrificial templates. A) Qualitative analysis of printability of 5–10 wt.% gelatin formulations, B) Upscaling of printed gelatin templates, and C) Demonstration of flexible print design of different shapes. D) Schematic overview of sacrificial printing process using conventional sacrificial ink (i.e., gelatin without Ru/SPS co-initiators) that display rapidly and without temporal control at the onset of cultivation, and using delayed dissolution sacrificial ink (i.e., gelatin with Ru/SPS co-initiators) that dissolve at a later time point during cultivation. E) Compatibility of a wide array of biomaterials to be used as bulk hydrogels for embedding of delayed dissolution sacrificial gelatin templates. F) EBP-enabled sacrificial printing as an off-the-shelf product, demonstrating the ability to freeze dry and rehydrate the constructs whilst retaining the delayed dissolution capacity of the sacrificial templates. G) Effect of SPS concentration in delayed dissolution gelatin inks on dissolution time of gelatin templates within the Gel-AGE bulk hydrogels. H) Microfluidics chips developed to investigate the use of multiple different delayed dissolution gelatin inks. I) Schematic of a printed gelatin template using two different delayed dissolution gelatin ink, which dissolved at two different time points as indicated by perfusion after J) 3 and 7 days. Scale bars = 1 mm. *N* = 3.

Table 1. Overview of nomenclature assigned to different sacrificial gelatin ink formulations.

	Sacrificial ink reference	Sacrificial ink formulation			Dissolution time [days]
		Gelatin [wt.%]	Ru [mm]	SPS [mm]	
Instant dissolution	SI-0	10	–	–	instant
Delayed dissolution	SI-1	10	0.1	3	1.0 ± 0.2
	SI-4	10	0.1	5	4.0 ± 1.0
	SI-11	10	0.1	7	10.7 ± 1.2
	SI-15	10	0.1	10	15.0 ± 1.0

sacrificial gelatin ink formulations. The number in the sacrificial ink nomenclature corresponds to their expected dissolution time. For example, SI-15 corresponds to sacrificial ink that dissolves after 15 days.

Gelatin templates without initiators (SI-0, Table 1) were used as control where rapid and temporally uncontrolled dissolution of the gelatin template upon incubation at physiological temperature (37 °C) was observed. Whilst we acknowledge that the SI-0 template dissolved rapidly at the onset of culture, rather than instant, the gelatin formulation without initiators was referred to as “instant dissolution” throughout the remainder of this work for brevity. Photo-cross-linked “delayed dissolution” templates were embedded within a secondary bulk hydrogel (Figure 3D), where it was hypothesized that the sacrificial templates will dissolve over time. For initial demonstration purposes, we selected S1-4 that was previously characterized to be dissolved completely after 4 days *in vitro*. It was demonstrated that S1-4 templates were successfully embedded within a range of bulk hydrogels that are of either synthetic or biological origin, such as methacrylated poly(vinyl alcohol) (PVA-MA), Gel-MA, Gel-AGE, Gel-NOR, and silk fibroin (Figure 3E). The mode of cross-linking, i.e., chain-growth polymerization (Gel-MA and PVA-MA) or step-growth polymerization (Gel-AGE and Gel-NOR) did not affect the embedding process. Furthermore, we were also able to show that the sacrificial templates were mechanically robust and easily adaptable to different cross-linking initiation methods. For instance, the bulk PVA-MA and Gel-MA hydrogels could be cross-linked either using photo-cross-linking (initiator + light) or redox-based cross-linking (N,N,N',N'-tetramethylethylenediamine/SPS). Additionally, the sacrificial templates could also be embedded within silk fibroin hydrogels that were cross-linked using methanol. Most importantly, dissolution of the S1-4 templates was achieved within all the various bulk hydrogels examined in this study. It is clearly seen from the cross-section images (Figure 3E) that open channels were present across all the constructs after 5 days of incubation. The application of EBP-enabled sacrificial printing to fabricate off-the-shelf constructs was also demonstrated. Constructs could be lyophilized and rehydrated at a later point without loss of structure, with the additional advantage of also retaining the delayed dissolution capacity of the embedded SI-4 templates (Figure 3F).

Sacrificial gelatin templates composed of SI-0, SI-1, SI-4, SI-11, and SI-15 were next embedded within bulk Gel-AGE hydrogels to investigate how the sacrificial template formula-

tion affected the timing of opening of microchannels within the bulk hydrogels. SI-0 templates dissolved at the onset of culture, an expected behavior of physically cross-linked gelatin. In contrast, SI-1, SI-4, SI-11, and SI-15 were still present within the bulk Gel-AGE hydrogels after 4 h of incubation (Figure S5, Supporting Information), but dissolved at later time points corresponding to their dissolution time as per Table 1 (Figure 3G). Crucially, this observation showed that sacrificial gelatin templates presented here can be used to introduce architectural cues within bulk hydrogels in a programmable, spatio-temporal manner. The temporal introduction of open channels into bulk hydrogels furthermore improved solute infusion (Figure S6, Supporting Information), which was expected given that previous studies have similarly demonstrated that the presence of microchannels in bulk hydrogels promotes solute infusion.^[6,7] Another attractive aspect of EBP-enabled sacrificial printing is the ability to combine multiple inks to allow the fabrication of constructs with spatially complex arrangements.^[45] We thus demonstrated that S1-4 and S1-11 could be co-printed and embedded within a single bulk hydrogel to facilitate complex dynamic perfusion once the templates dissolved (Figure 3H,I). Partial single-channel perfusion after 4 days of incubation was achieved due to dissolution of SI-4, whereas full dual-channel perfusion was observed after 11 days of incubation when both SI-4 and SI-11 had dissolved (Figure 3J).

While a large body of work exists on fabricating hydrogels with controllable degradability (e.g., using tyramine-functionalized poly(vinyl alcohol),^[27] N-(2-hydroxypropyl) methacrylate^[46] and N-isopropyl acrylamide^[47]) or macromers with degradable matrix metalloproteinases sequences), the use of these degradable hydrogels for sacrificial printing has to date only been investigated in a small number of studies.^[48,49] Murphy et al. developed an ink composed of star-shaped block co-polypeptides (poly(benzyl-L-glutamate)-b-oligo(L-valine)) that could be printed and cross-linked.^[48] These scaffolds demonstrated susceptibility to partial hydrolytic degradation over multiple weeks of culture (35–45% mass loss after 30 days, depending on the initiator concentration).^[48] Since these sacrificially printed constructs were developed with the aim of drug release in aqueous solution, the application of this sacrificial ink for fabricating microchannels within bulk hydrogels has not been explored to date. In another approach, Lutolf et al. enabled the dynamic introduction of physical features into hydrogels through laser ablation.^[50] Exposing poly(ethylene glycol) (PEG)-based hydrogels to short nanosecond pulsed lasers (80–150 mW) resulted in local breakdown of covalent bonds within the PEG polymer network, allowing the spatiotemporal introduction of channels within bulk hydrogels. Lutolf et al. were able to exploit this technique to generate intricate microfluidic channel networks within PEG hydrogels, albeit channel networks were limited to non-planar (i.e., 3D) structures. In this study, we demonstrated the spatio-temporal introduction of physical architectures in the form of 3D microchannel structures within bulk hydrogel constructs, using simple elegant chemistry. Temporal control over the introduction of physical features can be programmed, thus eliminating the need for post-fabrication manipulation of fabricated constructs. Moreover, our sacrificial templates are fabricated from easily available, pristine, non-chemically modified gelatin, combined with a visible light photo-initiating

system that has been previously proven to be more cytocompatible as compared to conventional UV-polymerization.^[31,51–53] The delayed dissolution of sacrificial gelatin templates is also expected to cause no cytotoxicity *in vitro* or *in vivo* as the degradation products (i.e., gelatin polypeptides) of these templates are generally considered safe.^[54]

2.3. Light-Based Sacrificial Printing of Delayed Dissolution Gelatin Inks

In recent years, light-based biofabrication platforms, such as DLP and VBP have been used to fabricate high-resolution hydrogel constructs.^[53] In DLP, a digital micromirror device is often used to generate a projection of light into a photo-

crosslinkable polymer, resulting in solidification of the polymer only in the regions of light exposure.^[55] VBP is another light-based biofabrication platform that enables rapid fabrication of complex 3D hydrogels by exposing a rotating vat of bioresin to a series of 2D projections, which combined together generate a 3D anisotropic optical light field within the volume of the photopolymer.^[56]

First, we investigated the application of DLP to fabricate delayed sacrificial gelatin templates followed by embedding of these templates in Gel-AGE bulk hydrogels (**Figure 4A**). S1-1, S1-4, S1-11, and S1-15 templates of varying dissolution rates were successfully fabricated at higher resolution (0.31 ± 0.08 mm) than EBP (Figure 4B; Figure S7, Supporting Information). Moreover, complex geometries, such as a snowflake and flower-like structure could be printed using DLP

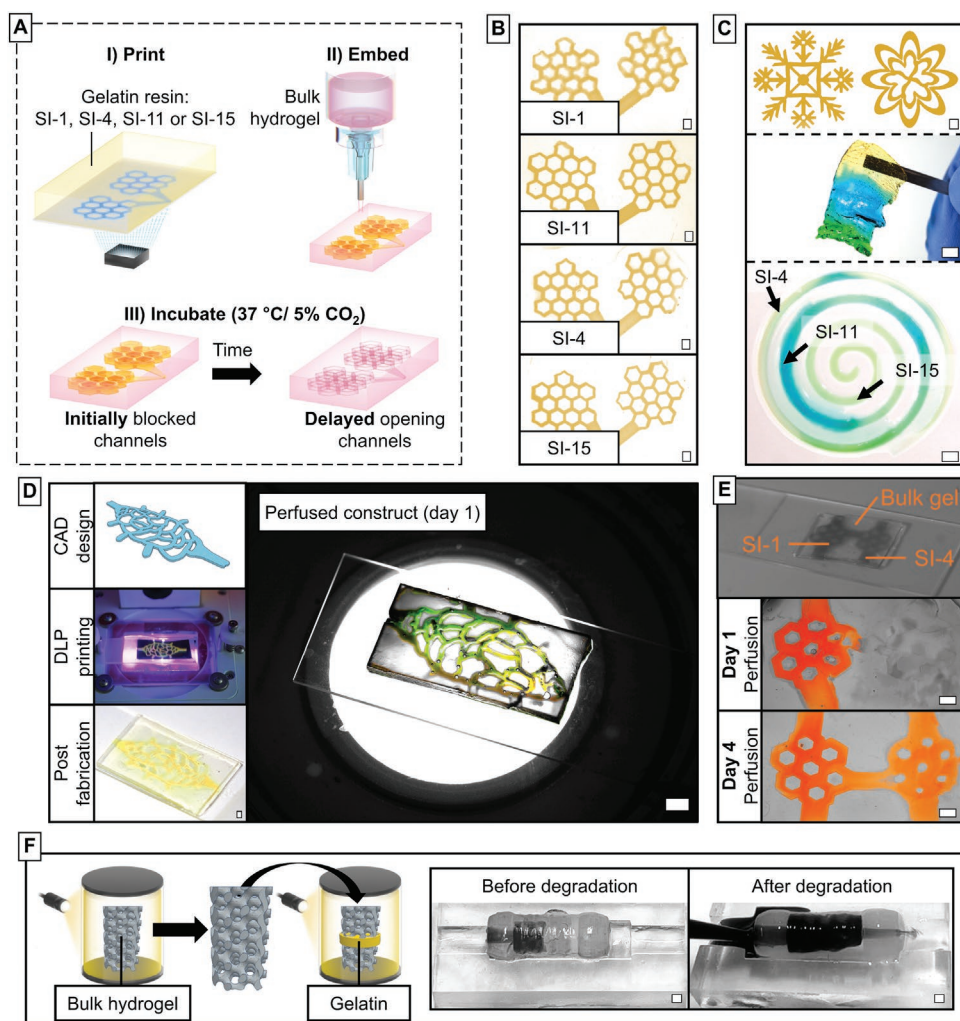


Figure 4. Light-based printing of sacrificial delayed dissolution gelatin inks. A) Schematic overview of DLP-enabled sacrificial printing. B) DLP-based fabrication of delayed dissolution sacrificial 10 wt.% gelatin templates with varying dissolution times. C) DLP-based fabrication of complex shapes and a hydrogel slab and spiral structure integrating various gelatin ink formulations containing no dye (S1-4), blue food coloring (S1-11), or green food coloring (S1-15). D) DLP-enabled sacrificial printing of structure (S1-1) resembling a vascular plexus and perfusion of the vascular plexus post template dissolution after 1 day of incubation. E) DLP-enabled fabrication of sacrificial gelatin templates with multiple delayed dissolution gelatin inks (S1-1 and S1-4) and subsequent embedding of templates in bulk hydrogels. Bulk hydrogels could be partially perfused after 1 day of incubation and fully perfused after 4 days of incubation. F) Two-step multi-material VBP-enabled sacrificial printing, consisting of VBP-enabled fabrication of a bulk hydrogel and subsequent VBP-enabled fabrication of a delayed dissolution sacrificial gelatin template within the bulk hydrogel. Scale bars = 1 mm. $N = 3$.

(Figure 4C). The snowflake structure contained smooth transitions filaments that varied in thickness (0.75–1 mm), which is a feature that would not be easily fabricated via EBP. Additionally, a flower-like structure was printed wherein the filament thickness gradually varied throughout each of the inner (0.6–2.5 mm) and outer (1–4 mm) petals. Another interesting capability that we demonstrated using DLP was the fabrication of a single template containing multiple gelatin formulations. We showed that three types of sacrificial inks could be spatially patterned in a spiral structure. For clearer visualization, we color-tagged the sacrificial inks, where SI-4, SI-11, and SI-15 were clear, blue, and green, respectively. The various sacrificial inks were integrated within a singular structure with smooth transitions at the interface (Figure 4C). Furthermore, we printed a vascular plexus-like structure using SI-1, which post-embedding and dissolution, resulted in open channels that could be readily perfused (Figure 4D). In another experiment, gelatin templates containing spatially defined regions composed of SI-1 and SI-4 were fabricated and embedded within a bulk Gel-AGE hydrogel (Figure 4E). On day 1, the SI-1 component of the sacrificial gelatin template dissolved, allowing partial perfusion of the bulk hydrogel with PBS-containing food dye. Only at day 4 could full perfusion be achieved as a result of delayed dissolution of the SI-4 component of the sacrificial gelatin template. Combining different sacrificial inks thus enables introduction of physical features within bulk hydrogels in a temporally controlled manner. DLP has only recently been used for the fabrication of sacrificial templates.^[49] Carberry et al. formulated a bioresin composed of thioester-functionalized PEG and norbornene-functionalized PEG, which could be processed through DLP, yielding high-resolution (<40 μm) features.^[49] While the authors were able to pattern bulk hydrogels on top of the sacrificial 2D patterns, the embedding of these patterns in bulk hydrogels to enable the fabrication of enclosed architectural elements was not possible. Moreover, degradation of their templates occurred within 2 h,^[49] as opposed to the wider range of dissolution rates (1–15 days) achievable using the gelatin sacrificial inks reported in this study.

While both DLP and EBP operate in a layer-by-layer fabrication process, respectively relying on the vertical displacement of a printing platform or of the extrusion needle, VBP is a layerless fabrication technique that manipulates and cross-links a whole volume of a bioresin in a contactless fashion (therefore, with no mechanical parts immersed or in contact with the material).^[53] As such, VBP can be used to non-invasively edit existing printed parts, by adding, for example, new architectures virtually anytime post-printing. Herein, we leveraged this possibility to introduce sacrificial structures within 3D-printed complex architectures. In this approach, VBP-enabled sacrificial printing was performed via a multi-material, sequential printing process, in which first a “bulk” hydrogel was fabricated in the form of a complex, centimeter-cube scaled gyroid, followed by a secondary step in which the sacrificial template was printed into the bulk hydrogel. In this proof-of-concept study, a bulk hydrogel was fabricated through VBP using a Gel-MA-based bioresin. In the second step, the Gel-MA gyroids were retrieved and immersed within a second bioresin composed of 15 wt.% gelatin and 0.3/50 mm/mm Ru/SPS. Using VBP, a secondary gelatin disc was printed to entangle across the

middle of the Gel-MA bulk hydrogel (Figure 4F). Prior to dissolution of the sacrificial template, the gelatin disc served as a plug, preventing full perfusion of the gyroid. After dissolution of the sacrificial template, full perfusion of the bulk hydrogel was possible (Figure 4F). This proof-of-concept study demonstrated the feasibility of using VBP-enabled sacrificial printing for the rapid generation of well-defined 3D constructs with dynamically tuneable perfusion.

EBP is an attractive platform as it is widely available, relatively low-cost, and allows layer-by-layer deposition of spatially well-defined structures as demonstrated in this paper. On the other hand, DLP offers a higher resolution (ranging between 5–50 μm)^[53,57,58] than EBP as well as the capability of fabricating complex structures. In our previous studies, we used DLP to fabricate woven and chainmail-like hydrogel structures, as well as bulk hydrogels with complex microchannels.^[17,59] More recently, we also developed a DLP system that enabled printing of different structures with a 49 μm of resolution using a range of resins, such as poly(ethylene glycol)-diacrylate (PEGDA), Gel-MA, and Gel-AGE.^[60] With respect to VBP, its major advantage over EBP and DLP lies in its ability to generate constructs with complex elements, such as overhangs or well-defined porous structures with fabrication speeds that exceed those of other biofabrication techniques.^[18,56,61] Bernal et al. showed that perfusable hydrogel-based constructs can be VBP-printed in under 15 s, whereas EBP of similar constructs requires 25 min.^[56] Taken together, our results demonstrated for the first time the possibility of using light-based printing platforms, such as DLP and VBP to fabricate sacrificial templates of tuneable dissolution rates. The ability of the delayed dissolution sacrificial gelatin inks to be applied across EBP, DLP, and VBP highlights the versatility of this elegant platform. Pristine, non-chemically modified gelatin is also readily available, requiring no lengthy chemical synthesis protocols. As a result, these inks can be easily adopted by researchers and applied across various biofabrication platforms. This versatility is of particular significance as each of these biofabrication techniques are further associated with different resolution, printing speed, and template designs, which can now be spatially and temporally introduced into bulk hydrogel constructs.

2.4. Effect of Delayed Introduction of Microchannels Within Cell-Laden Bulk Hydrogels on Osteogenic Differentiation of Encapsulated Cells

The previously characterized 3D-printed sacrificial templates with unique delayed dissolution capabilities allowed spatial and temporal control over the introduction of physical architectures within large-scale hydrogel constructs. This platform opens up the possibility to present cells within hydrogel constructs with spatio-temporally well-defined microenvironments, that may modulate their behavior and functionality. In our first proof-of-concept example, we applied these delayed-dissolution sacrificial templates to mesenchymal stromal cell (MSC)-laden Gel-AGE constructs that were cultured in osteogenic media to target bone engineering. Sacrificial templates with instant dissolution (SI-0), rapid delayed dissolution (SI-4: 4 days), and slow delayed dissolution (SI-15: 15 days) were incorporated

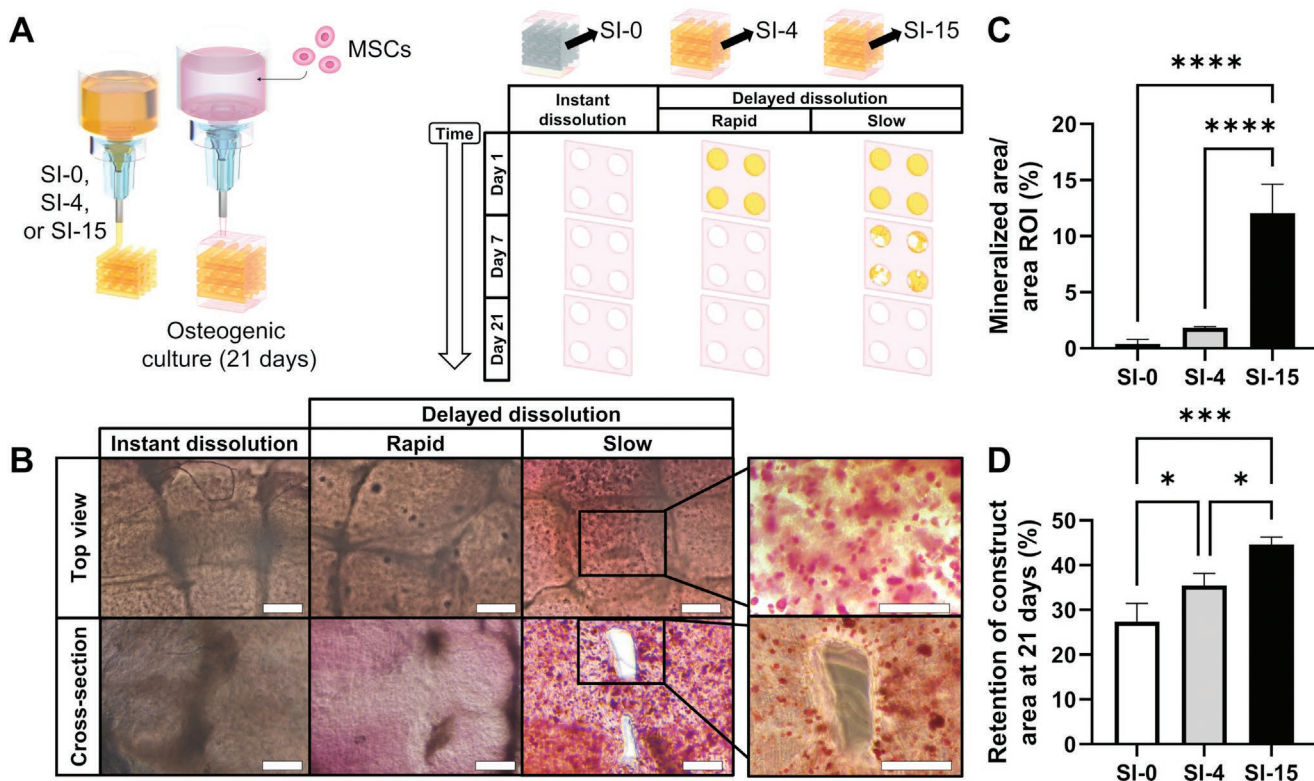


Figure 5. Osteogenesis in bulk Gel-AGE hydrogels with delayed dissolution sacrificial gelatin templates. A) Schematic overview of experimental setup, investigating the effect of the timing of gelatin template dissolution on mineralization within bulk MSC-laden ($5 \text{ million mL}^{-1}$) Gel-AGE hydrogel constructs after 21 days of culture. B) Effect of gelatin template dissolution rate on mineralization as visualized through Alizarin Red (red) staining at day 21 of culture. C) Quantification of percentage area change as compared to the initial construct area at day 21. D) Quantification of construct mineralization as calculated through the percentage of area with positive Alizarin Red staining compared to the total construct cross-sectional area. Scale bars = 1 mm. One-way ANOVA with post hoc Tukey test between experimental groups. Statistical differences are depicted by * ($p < 0.05$), *** ($p < 0.001$), and **** ($p < 0.0001$), $N = 3$.

into bulk MSC-laden Gel-AGE hydrogels (2.7 mm in thickness) to introduce open microchannels through EBP-enabled sacrificial printing (Figure 5A). These sacrificial templates were selected in accordance to relevant timeframes for osteogenesis (2–3 weeks)^[62] as previously reported in the literature. Bulk hydrogel discs (8 mm × 8 mm × 2.7 mm) without microchannels were used as controls. We observed that MSCs within Gel-AGE constructs without microchannels showed limited osteogenesis/mineralized module formation ($0.33 \pm 0.39\%$ mineralization of the total construct area, Figure S8A,B, Supporting Information). This result is expected as previous reports have observed limitations in passive diffusion of oxygen and nutrients, which negatively impacted cell functionality.^[63,64] Surprisingly, the instant dissolution group (SI-0) also showed close-to-no mineralization (Figure 5B), with mineralization occurring in only $0.4 \pm 0.4\%$ of the total construct area (Figure 5C). Slightly delaying the dissolution rate of the sacrificial templates to 4 days (SI-4) seemingly improved mineralization (Figure 5B), albeit the increase in the area of mineralization ($1.8 \pm 0.1\%$) was not significant (Figure 5C). Most interestingly, further delaying the dissolution of the sacrificial template to 15 days (SI-15) resulted in significantly increased mineralization ($12.1 \pm 2.6\%$) from MSCs encapsulated within the large-sized bulk Gel-AGE hydrogels (Figure 5B,C).

Furthermore, we observed that over the culture period, construct shrinkage (defined as the percentage retention of the initial construct area) was observed in all experimental groups (Figure 5C,D). It should be noted that constructs with no cells did not contract (Figure S8C, Supporting Information), validating that construct contraction was indeed cell-mediated. We believe that as MSCs can interact with the Gel-AGE network through the abundance of native RGD sequences, the resultant cell-polymer interaction was able to lead to contractile forces that caused the overall construct to shrink.^[65] After 21 days of culture, the instant dissolution group (SI-0) shrunk significantly, retaining only $27.4 \pm 4.1\%$ of its initial construct area (Figure 5D). As the constructs were shrinking, we also observed that channel closure occurred, where no open channels could be seen on day 21 (Figure 5B). Delaying the dissolution of the sacrificial templates significantly reduced the extent of contraction. After 21 days of culture, the retention values of the initial construct areas were $35.9 \pm 2.7\%$ and $44.6 \pm 1.6\%$ for the rapid (SI-4) and slow (SI-15) delayed-dissolution samples, respectively (Figure 5D). Thus, it is shown that the physical barrier provided by the delayed-dissolution sacrificial gelatin template seemingly mitigated channel closure otherwise occurring with instant dissolution.

We hypothesize that the different degree of mineralization observed within the different samples was due to the variation

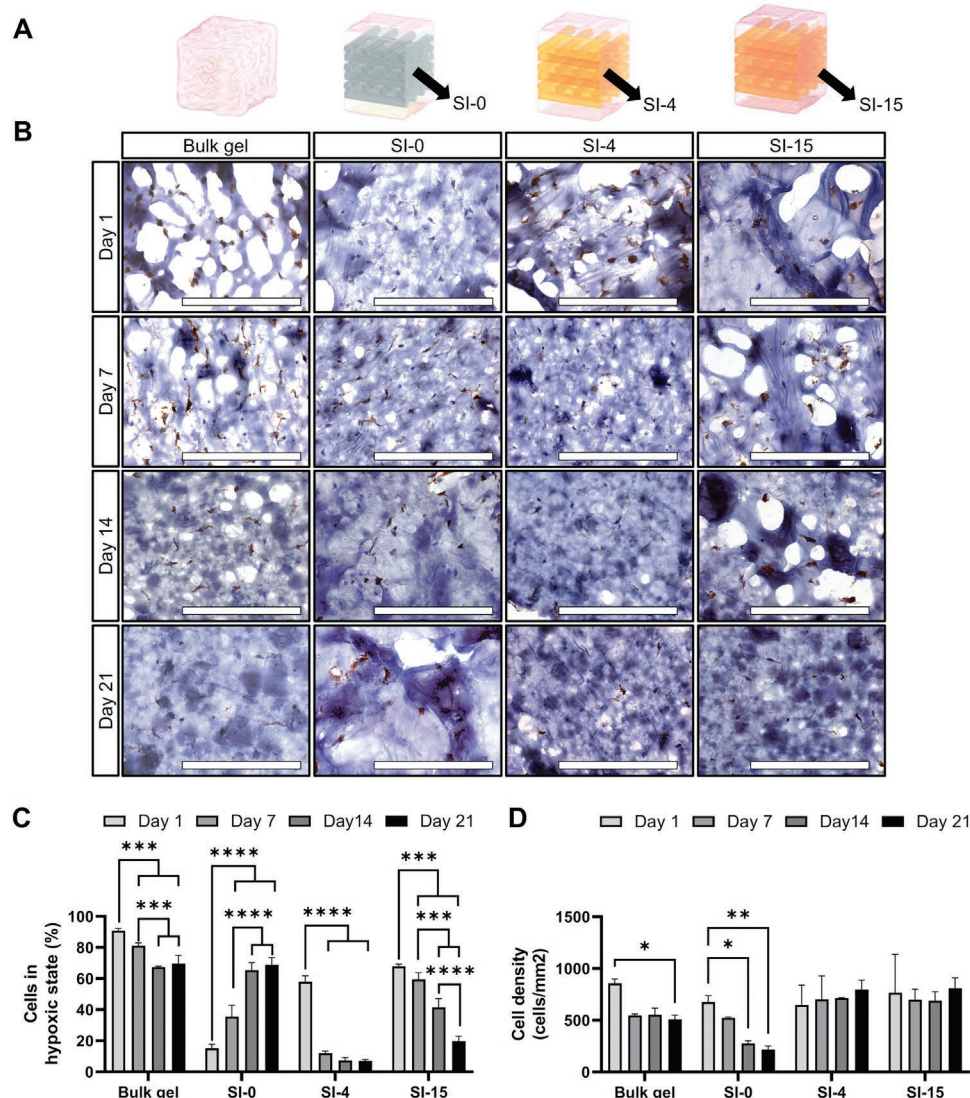


Figure 6. Effect of timing of delayed dissolution sacrificial gelatin template on solute availability to cells within osteogenically cultured bulk Gel-AGE hydrogels. A) MSCs ($5 \text{ million mL}^{-1}$) was encapsulated in bulk hydrogels ($8 \text{ mm} \times 8 \text{ mm} \times 2.7 \text{ mm}$), containing no channels, an instantly dissolving sacrificial gelatin template (SI-0), and two different formulations of delayed dissolving sacrificial gelatin templates (SI-4 and SI-15). B) Representative images of construct cross-sections stained for pimonidazole (brown) to stain cells in hypoxic state and hematoxylin (blue). C) Quantification of the percentage cells in hypoxic state in the three experimental groups after 1, 7, 14, and 21 days of culture. D) Quantification of the cell density in the three experimental groups after 1, 7, 14, and 21 days of culture. Scale bars = $200 \mu\text{m}$. One-way ANOVA with post hoc Tukey test between experimental groups. Independent sample *t*-tests between different time points within one experimental group. Statistical differences are depicted by * ($p < 0.05$), ** ($p < 0.01$), *** ($p < 0.001$), and **** ($p < 0.0001$), $N = 3$.

in oxygen availability presented to MSCs encapsulated within the hydrogel constructs. This hypothesis was further investigated through characterization of the dynamic changes in cell hypoxic state in response to the timing of introduction of microchannels within MSC-laden Gel-AGE hydrogels. In this study, we used instantly dissolution (SI-0) and two different formulations of delayed dissolution (SI-4 and SI-15) sacrificial templates, which were embedded within the MSC-laden bulk hydrogels (Figure 6A). Bulk hydrogels ($8 \text{ mm} \times 8 \text{ mm} \times 2.7 \text{ mm}$) with no microchannels were used as controls. These constructs were incubated in media containing pimonidazole to investigate the hypoxic state of cells.

When cells are experiencing low local oxygen concentrations ($<1.3\% \text{ O}_2$),^[64] pimonidazole is covalently incorporated within cells, allowing visualization of these hypoxic cells through immunohistochemical analysis (Figure 6B). Bulk hydrogels without channels had limited oxygen permeability, resulting in a consistently higher percentage of hypoxic cells ($\approx 80\%$ throughout all time points, Figure 6C). Interestingly, when microchannels were introduced into the Gel-AGE hydrogel constructs in the instant dissolution group, only a low number of hypoxic cells were present at day 1 ($15.2 \pm 2.6\%$), but the number of hypoxic cells gradually increased significantly over time to $35.6 \pm 7.3\%$ (day 7), $65.5 \pm 4.7\%$ (day 14) and $68.9 \pm 4.5\%$

(day 21). This phenomenon was likely a consequence of the cell-mediated construct contraction, where the cell-hydrogel interaction led to complete closure of the introduced microchannels (Figure 6B,C). In contrast, the SI-4 group provided an initial hypoxic environment within the bulk hydrogel as evidenced by a high percentage of hypoxic cells ($58.1 \pm 3.6\%$) on day 1. This result is expected due to the fact that if the SI-4 templates within the Gel-AGE construct had not dissolved, the overall construct should behave similarly to the bulk hydrogel control without microchannels. Interestingly, the percentage of hypoxic cells in the delayed dissolution group decreased significantly to $12.1 \pm 1.4\%$ after 7 days of culture. This low percentage of hypoxic cells ($7.3 \pm 1.8\%$ on day 7 and $7.0 \pm 0.9\%$ on day 21) within the SI-4 group was maintained for the remainder of the culture period of 21 days. The SI-15 group followed a similar trend to the SI-4 group. Initially, a high percentage of hypoxic cells ($67.9 \pm 1.3\%$) was observed on day 1. Over the culture period of 21 days, the percentage of hypoxic cells reduced to $59.4 \pm 4.3\%$, $41.5 \pm 5.7\%$, and $19.8 \pm 3.1\%$ for 7, 14, and 21 days, respectively. It is also interesting to note a reduction in the total cell density could be observed in the bulk hydrogels that contained no channels, as well as the bulk hydrogels in the instant-dissolution samples (Figure 6D). In contrast, the cell density in the delayed dissolution samples remained stable, suggesting that the prolonged increase in percentage of hypoxic cells in the bulk hydrogel and instant-dissolution samples may have caused cell death over the culture period of 21 days. These results verified that by controlling the dissolution rate of the sacrificial templates, we are able to modulate the oxygen availability within regions of the hydrogels, which can further direct cellular function.

The effect of hypoxia on in vitro and in vivo bone formation is not fully understood with a body of work showing conflicting results.^[66,67] Recent studies however suggest that oxygen regulation could serve to promote osteogenesis depending on the oxygen profile during culture.^[68–71] In one study, MSCs were expanded in a hypoxic environment prior to encapsulation within a hydrogel blend of alginate and decellularized bone matrix. Hypoxia-induced MSCs expressed higher levels of osteocalcin, a late bone differentiation marker. These effects were attributed to an increased hypoxia-inducible factor 1- α expression, causing an upregulation of the AKT/mTOR signaling pathway which is associated with increased cell proliferation and metabolism.^[68] Another study revealed the importance of the duration of hypoxia in regulating osteogenesis. MSCs were cultured in hypoxic conditions (3% O₂) for 1, 3, 5, or 7 days, prior to switching to normoxic conditions for the remainder of the 7 days culture period. Osteogenic markers, such as collagen type I and alkaline phosphatase were upregulated when exposing MSCs to 3 days of hypoxia compared to a normoxic control, while this effect was not observed in MSCs exposed to hypoxia for 1, 5, or 7 days.^[69] Taken together, it is clear that temporal variations in local oxygen concentrations (i.e., the progression in the percentage of hypoxic cells over time) play a vital role in regulating osteogenesis. More specifically, our results indicate that the relationship between the timing/duration of hypoxia and the differentiation stage of encapsulated MSCs is vital in steering mineralization. With that in mind, the delayed dissolution sacrificial gelatin platform provides a valuable tool

within bone tissue engineering by enabling the temporal control over the microenvironmental cues (i.e., oxygen availability, nutrient supply) in engineered constructs.

2.5. Effect of Delayed Introduction of Microchannels Within Cell-Laden Hydrogels on Formation of Capillary-Like Network

Our delayed sacrificial printing technology was further investigated in neo-vascularization applications. Instant-dissolution (SI-0), rapid delayed-dissolution (SI-1: 1 day), and slow delayed-dissolution (SI-4: 4 days) templates were embedded within bulk Gel-AGE hydrogels containing green fluorescent protein expressing human umbilical vein endothelial cells (GFP-HUVECs) and MSCs (Figure 7A). These templates were selected in accordance to dissolution rates that are relevant to neo-vascularization timeframes (1–2 weeks).^[72]

In general, it was observed that the Gel-AGE hydrogel provided a permissive environment for the GFP-HUVECs to self-assemble into capillary-like networks (Figure 7B; Figure S9, Supporting Information). After 10 days of culture, capillary-like structures were clearly visible in cross-sections of all constructs, where spreading of endothelial cells (cluster of differentiation 31; CD31, green) and pericyte-like cells (α SMA, red) was observed. Interestingly, the extent of capillary-like network formation was significantly affected by the dissolution rate of the sacrificial templates. While the instant dissolution group facilitated the formation of capillary-like networks with an average vessel length of 0.085 ± 0.014 mm, delaying the opening of the microchannels for just 1 day (SI-1, rapid dissolution) already resulted in significantly longer average vessel length of 0.131 ± 0.015 mm. In addition, further delaying the dissolution of the sacrificial templates to 4 days significantly increased the average vessel length to 0.271 ± 0.025 mm (Figure 7C). A similar trend was obtained with the quantification of vessels junction density, whereby delaying the opening of the microchannels resulted in higher junction density (Figure 7D).

In native tissues, capillaries are found no further than 150–200 μ m from surrounding cells to ensure adequate oxygen and nutrient availability to cells as well as ensure efficient waste removal.^[72] Therefore, without the presence of open microchannels within the bulk Gel-AGE hydrogels, passive diffusion across the periphery of the construct is insufficient to ensure adequate oxygen and nutrient delivery to the hydrogel core.^[62] As shown in Figure 6, delaying the sacrificial template dissolution served as a method to introduce dynamic variations in oxygen and nutrient supply across MSC-laden Gel-AGE hydrogels. Similarly, delaying the dissolution of the sacrificial template enabled the introduction of dynamic variations in oxygen and nutrient supply during the cellular self-assembly of encapsulated MSCs and HUVECs to capillary-like networks in this experiment (Figure 8). In contrast to the MSC-laden Gel-AGE hydrogels cultured under osteogenic conditions (Figures 5 and 6), limited cell-mediated contraction was observed in all experimental groups in the neovascularization studies. As a result, a stable normoxic environment was maintained in the SI-0 group as evidenced by a low number of hypoxic cells present in this group throughout the entire culture period ($14.4 \pm 2.4\%$, $13.3 \pm 1.8\%$ and $14.7 \pm 1.0\%$ for 1, 3, and 10 days,

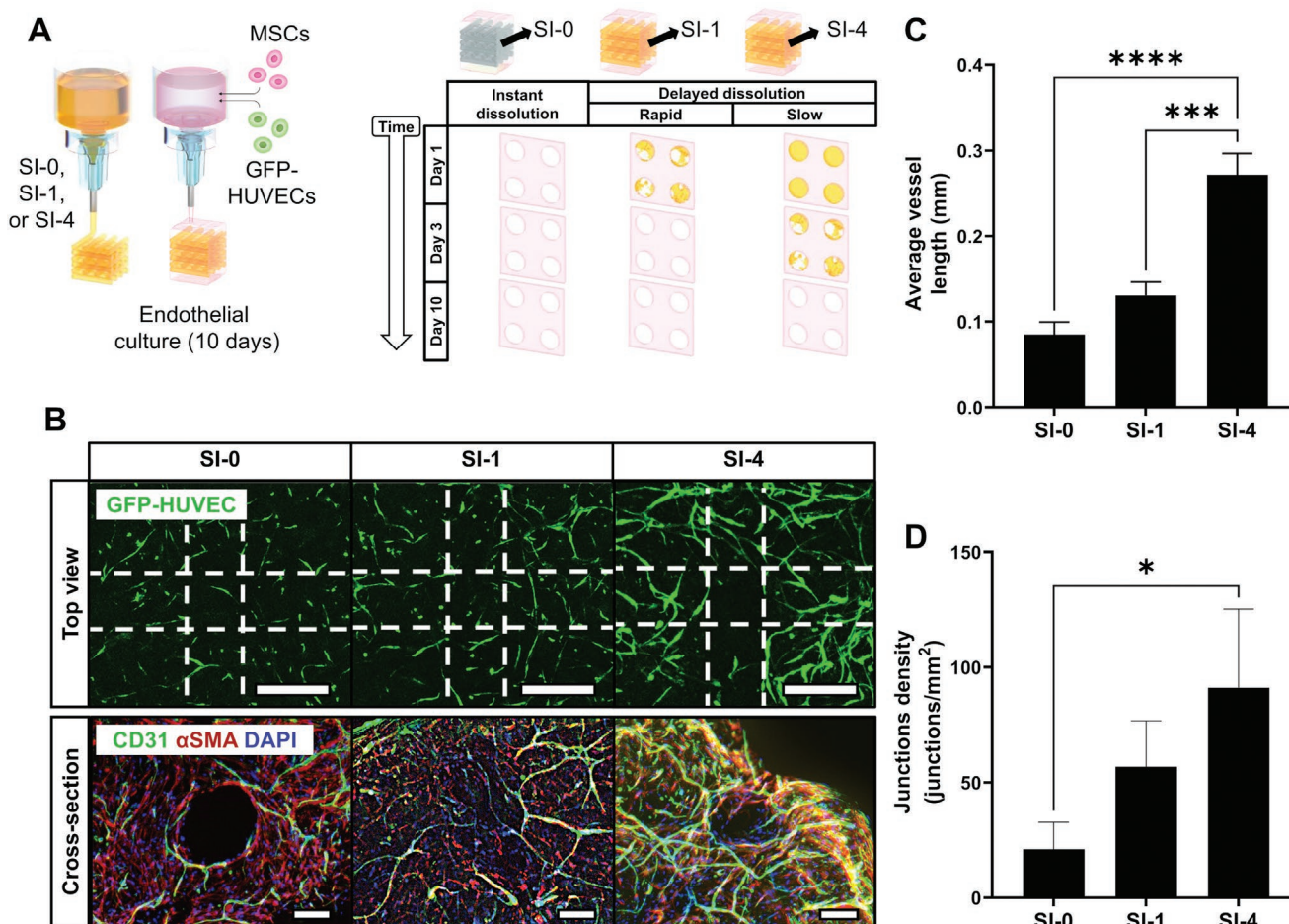


Figure 7. Capillary-like network formation in bulk Gel-AGE hydrogels with delayed dissolution sacrificial gelatin templates. A) Schematic overview of experimental setup, investigating the effect of the timing of gelatin template dissolution on capillary-like network formation within bulk GFP-HUVEC-laden ($2.5 \text{ million mL}^{-1}$) and MSC-laden ($2.5 \text{ million mL}^{-1}$) Gel-AGE hydrogel constructs after 10 days of culture. B) Effect of gelatin template dissolution rate on capillary-like network formation as visualized through GFP+ signal at day 10 of culture, as well as representative immunohistochemistry of construct cross-sections, showing CD31 (green), α SMA (red) and DAPI (blue) around construct channels at day 10 of culture. C,D) Quantification of capillary-like network formation at day 10 of culture. Scale bars = 1 mm. One-way ANOVA with post hoc Tukey test between experimental groups. Statistical differences are depicted by * ($p < 0.05$), *** ($p < 0.001$), and **** ($p < 0.0001$), $N = 3$.

respectively, Figure 8C). In contrast, the SI-1 group initially provided a hypoxic environment ($37.4 \pm 1.9\%$ hypoxic cells at day 1), but provided a normoxic environment for encapsulated cells after template dissolution ($22.2 \pm 8.4\%$ and $21.0 \pm 5.9\%$ hypoxic cells at 3 and day 10, respectively). Similarly, the SI-4 group demonstrated a hypoxic environment prior to template dissolution ($60.7 \pm 6.1\%$ and $59.8 \pm 4.7\%$ hypoxic cells at 3 and day 10, respectively) and a normoxic environment after template dissolution ($17.8 \pm 4.9\%$ hypoxic cells at day 10). Oxygen tension is a well-known regulator of neo-vascularization through cellular self-assembly of MSCs and HUVECs.^[73,74] One report investigated endothelial cells, that when seeded onto collagen gels, showed increased sprouting into the collagen gel under hypoxic conditions as compared to normoxic conditions.^[73] Another report demonstrated that reducing oxygen concentration to 1% reduced angiogenic sprouting of endothelial cells seeded on top of fibrin hydrogels.^[74] It is therefore likely that the enhanced capillary-like network formation within the delayed dissolution samples was due to the temporally reduced oxygen availability.

Considering the significant effect these temporal changes had on capillary-like network formation, the delayed dissolution sacrificial gelatin ink platform provides an invaluable tool to investigate the specific temporal demands on oxygen and nutrients required for optimal capillary-like network formation for application in pre-vascularization strategies.

A limitation of traditionally used sacrificial inks, such as Pluronic F-127 or carbohydrate glass, is the inability of these inks to incorporate or deliver cells within them in a cytocompatible manner. In contrast, gelatin sacrificial inks described herein are cytocompatible due to their water solubility and abundance of cell-interactive motifs. We, therefore, investigated the possibility of delivering cells within the sacrificial gelatin templates in a dynamic manner. A key aspect of this approach however is the successful interaction of cells within the sacrificial gelatin compartment and cells encapsulated within the bulk hydrogel. Here, GFP-HUVEC-laden sacrificial templates were incorporated within bulk Gel-AGE hydrogels containing MSCs (Figure 9A).

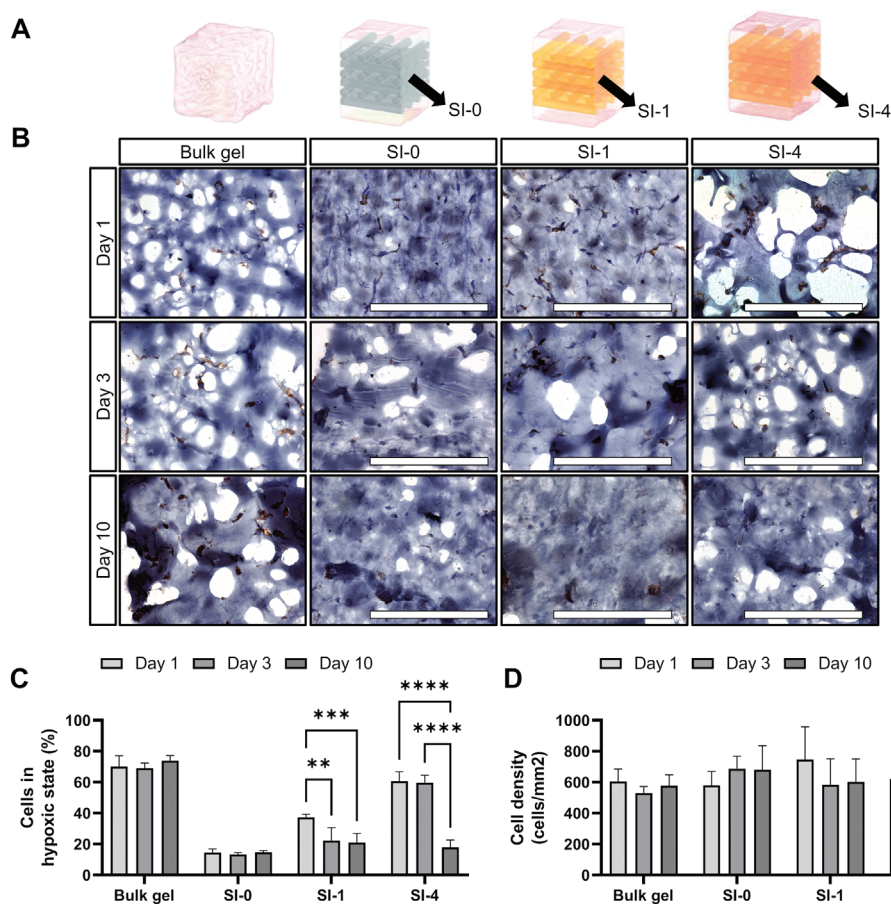


Figure 8. Effect of timing of delayed dissolution sacrificial gelatin template on solute availability to cells within vascular cultured bulk Gel-AGE hydrogels. A) A co-culture of MSCs and HUVECs ($2.5 \text{ million mL}^{-1}$ each) was encapsulated in bulk hydrogels ($8 \text{ mm} \times 8 \text{ mm} \times 2.7 \text{ mm}$), containing no channels, an instantly dissolving sacrificial gelatin template (SI-0), and two different formulations of delayed dissolving sacrificial gelatin templates (SI-1 and SI-4). B) Representative images of construct cross-sections stained for pimonidazole (brown) to stain cells in hypoxic state and hematoxylin (blue). C) Quantification of the percentage cells in hypoxic state in the three experimental groups after 1, 3, and 10 days of culture. D) Quantification of the cell density in the three experimental groups after 1, 3, and 10 days of culture. Scale bars = $200 \mu\text{m}$. One-way ANOVA with post hoc Tukey test between experimental groups. Independent sample *t*-test between different time points within one experimental group. Statistical differences are depicted by ** ($p < 0.01$), *** ($p < 0.001$), and **** ($p < 0.0001$), $N = 3$.

Based on the previous characterization of endothelial cell behavior (Figure 7), SI-4 was selected as the delayed dissolution sacrificial ink formulation. This formulation was further supplemented with poly(vinyl alcohol) (PVA, 1.5 wt.%) that served as a porogen.^[75,76] Increasing porosity can improve cell spreading and motility,^[75,77] potentially aiding cellular interaction across the interface of the sacrificial template and bulk hydrogel. Mass loss and swelling studies revealed that addition of PVA to the SI-4 templates resulted in a significant increase in sol fraction (Figure 9B), due to the leaching of PVA out of the gelatin hydrogel template.^[75,76] During this process, micropores were formed within the SI-4 templates, which also resulted in an increased swelling ratio (Figure 9C). It should be noted that the use of a porogen to impart microporosity within a sacrificial hydrogel network is not possible in conventional sacrificial inks, such as Pluronic F-127 or carbohydrate glass given that they instantly dissolve without any hydrogel network remaining (data not shown). Thus, the ability to introduce porogens within sacrificial gelatin templates and the subsequent embedding of

these templates within bulk Gel-AGE hydrogels to introduce a dynamic physical cue is a unique feature of the technology reported here.

In the instant dissolution group, both MSCs (αSMA , red) and GFP-HUVECs (CD31, green) were randomly distributed within the constructs after 10 days of culture, with very limited microcapillary network observed (Figure 9D). Interestingly, HUVECs were able to align along the microchannels introduced via the delayed sacrificial templates (Figure 9D). The average vessel length and junctions density of formed capillaries were significantly higher within the channels of the delayed dissolution samples (Figure 9E,F). The delayed dissolution group also showed improved co-localization of the two compartmentalized cell populations. The presence of αSMA -positive MSCs around the endothelial structures is significant, as these MSCs act as pericyte-like cells that stabilize the formed endothelial network.^[14,78] After 10 days of culture, dense MSC elongations could be observed around the channels outlined with gridlines, whilst HUVECs aligned within the construct

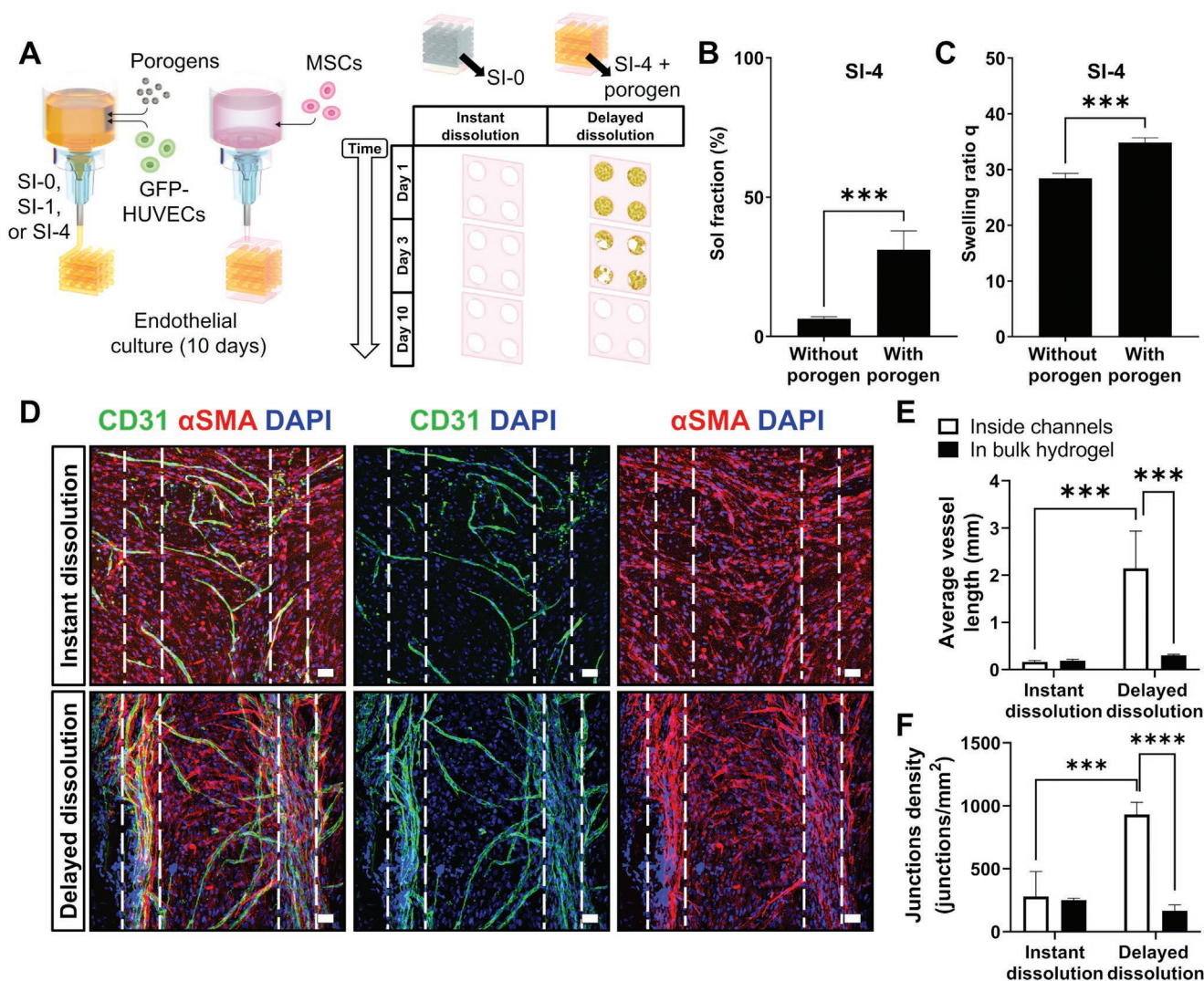


Figure 9. Compartmentalization of stromal cells in bulk Gel-AGE hydrogels and endothelial cells in delayed dissolution sacrificial gelatin templates. A) Schematic overview of experimental setup, investigating the effect timing of gelatin template dissolution on behavior of GFP-HUVECs ($2.5 \text{ million mL}^{-1}$) that were encapsulated within sacrificial gelatin templates and MSCs ($2.5 \text{ million mL}^{-1}$) that were encapsulated in bulk Gel-AGE hydrogels. B,C) Effect of addition of porogens to delayed dissolution sacrificial gelatin formulations on mass loss and mass swelling properties of the hydrogels after overnight incubation. D) Behavior of endothelial and stromal cell types within bulk hydrogels and channels (outlined with gridlines) after 10 days of culture. Representative immunohistochemistry pictures of construct cross-sections, showing endothelial cells through CD31 expression (green), and stromal cells through α SMA (red). Nuclei were stained with DAPI (blue). E,F) Quantitative analysis of the capillary-like network formation occurring within construct channels and within bulk hydrogel after 10 days of culture. Scale bars = 1 mm. One-way ANOVA with post hoc Tukey test between experimental groups. Statistical differences are depicted by *** ($p < 0.001$) and **** ($p < 0.0001$), $N = 3$.

channels (Figure 9D). As MSCs were only initially encapsulated within the bulk Gel-AGE region, it is therefore apparent that the MSCs were able to migrate into the embedded sacrificial gelatin template/channel. Hydrogel porosity is known to play a major role in governing cell movement.^[79] A previous study demonstrated that MSCs could infiltrate into a poly(lactic acid) hydrogel with pore sizes as small as $65 \mu\text{m}$.^[80] Therefore, it is likely that the inclusion of the PVA porogen into the delayed dissolution sacrificial gelatin biopinks allowed the fabrication of templates with sizeable pores to allow cell infiltration of MSCs and GFP-HUVECs across the channel-gel interface, hence improving cellular interactions across this interface. In this study, capillary-like network formation was facilitated through

the spatio-temporally controlled transition from porous to open microchannels within the bulk hydrogel, which is enabled only through the combination of the delayed dissolution sacrificial gelatin ink and porogen leaching platforms.

3. Conclusion

By exploiting the unique ability of the visible light Ru/SPS photo-initiating system to crosslink native tyrosine moieties present in gelatin, pristine gelatin could be photo-cross-linked into loosely cross-linked hydrogel with tailorable and programmable dissolution rates (1–15 days). These gelatin-based

sacrificial inks were applied across a range of biofabrication modalities (EBP, DLP, VBP), where sacrificial gelatin templates with customizable dissolution rates were successfully fabricated. These templates were versatile and could be embedded within a range of bulk hydrogels composed of various materials and different cross-linking chemistries. Spatio-temporal introduction of physical architectures within these hydrogel constructs was further achieved, where microchannels can be controlled to open at various time frames ranging from 1 to 15 days depending on the formulation of gelatin sacrificial ink. This approach allowed modulation of the hydrogel microenvironment (i.e., oxygen availability), and was proven to be a useful strategy to direct cell function, including osteogenesis and capillary-like network formation. Further compartmentalization of GFP-HUVECs within the delayed dissolution gelatin templates and MSCs within the bulk Gel-AGE hydrogels, allowed spatial control of vessel formation and an alignment of formed capillaries within the fabricated channels. Overall, these results highlighted the importance of replicating dynamic processes that occur in native tissue formation, maturation, and homeostasis. With this in mind, the presented delayed dissolution sacrificial gelatin ink platform provided a tool that has the unique capacity to spatio-temporally introduce architectural cues within bulk hydrogels. As this platform is based on pristine, non-chemically modified gelatin, it can be easily adopted by the wider scientific community and applied to the wide range of biofabrication modalities presented in this paper. This platform for instance allows researchers to investigate how dynamic physical cues play a role in the development of a wide range of tissue types and exploit temporal changes in the physical microenvironment of tissue substitutes to augment tissue formation. Additionally, the incorporation of more complex spatio-temporal variations in the presentation of physical cues (i.e., through combining multiple delayed dissolution sacrificial gelatin ink formulations) will enable further investigations into native tissue processes. We believe that this technology thus offers wide applicability within the biofabrication, tissue engineering, and regenerative medicine fields.

4. Experimental Section

Materials: Porcine skin type A gelatin (bloom strength 300 g), 13–23 kDa poly(vinyl alcohol) (PVA) for macromer synthesis, 146–186 kDa PVA as porogen, methacrylic anhydride, allyl glycidyl ether (AGE), carbic anhydride, phosphate-buffered saline (PBS) tablets, sodium hydroxide (NaOH), concentrated hydrochloric acid (HCl), sodium hydroxide (NaOH), cellulose membrane dialysis tubing, lithium bromide, sodium carbonate, tris(2'-2'-bipyridine)dichloro-ruthenium(II) hexahydrate (Ru), sodium persulfate (SPS), dithiothreitol (DTT), N,N,N',N'-tetramethylethylenediamine (TEMED), L-ascorbic acid-2-phosphate sesquimagnesium salt (AsAp), β -glycerophosphate (β -GP), dexamethasone (Dex), sodium azide (SA), Triton X-100, 12–14 kDa molecular weight cut-off (MWCO) dialysis membrane, alizarin Red S solution (pH 4.2), 4% neutral buffered formaldehyde, alcian blue were obtained from Sigma-Aldrich (MO, USA). Irgacure 2959 (Irg2959), or 2-Hydroxy-4'-(2-hydroxyethoxy)-2-methylpropiofenone was obtained from BASF. lithium phenyl-2,4,6-trimethylbenzoylphosphine was purchased from TCI Chemicals (Japan). Gibco α MEM media, penicillin-streptomycin (10 000 units mL⁻¹, PS), Gibco fetal bovine serum (FBS), Gibco trypsin, and Coomassie Plus Assay Reagent were obtained

from Thermo Scientific (New Zealand). Basic fibroblast growth factor (bFGF), primary mouse anti-human cluster of differentiation 31 (CD31) antibody and primary rabbit anti-human alpha-smooth muscle actin (α SMA) antibody were purchased from R&D Systems (MN, USA). Secondary fluorescein isothiocyanate (FITC)-conjugated goat anti-mouse antibody was purchased from Life Technologies (CA, USA). Secondary tetramethyl rhodamine (TRITC)-conjugated donkey anti-rabbit antibody was purchased from Abcam (Australia). Vascular cell basal media, endothelial cell growth kit-VEGF, trypsin for primary cells, and trypsin neutralizing solution were purchased from ATCC (VA, USA). Pimnidazole hydrochloride, FITC-labeled anti-pimnidazole mouse IgG1 monoclonal antibody, and HRP-conjugated anti-FITC rabbit antibody were purchased from Hypoxyprobe Inc (MA, USA).

Macromer Synthesis and Characterization: Methacrylated poly(vinyl alcohol) (PVA-MA) was synthesized according to the published protocol.^[59] PVA (10 wt.%) was dissolved in deionized water at 80 °C. After dissolution, the PVA solution was allowed to cool down, after which methacrylic anhydride was added (0.39 g gelatin). The reaction was maintained at room temperature for 48 h. Afterward, the pH of the reaction mixture was adjusted to eight. Methacryloyl-functionalized gelatin (Gel-MA) was synthesized according to the published protocol.^[31] Gelatin (10 wt.%) was dissolved in deionized water at 50 °C and methacrylic anhydride was added (0.6 g g⁻¹ gelatin). The reaction was maintained at 50 °C for 1 h. Afterward, the reaction was quenched by 3x dilution in deionized water. The reaction mixture was finally centrifugated, removing the solute fraction containing unreacted methacrylic anhydride. Allyl-functionalized gelatin (Gel-AGE) was synthesized according to published protocol.^[11] Briefly, gelatin (10 wt.%) was dissolved in deionized water at 65 °C. AGE and NaOH (2.4 and 0.4 mmol g⁻¹ gelatin, respectively) were added after which the reaction was maintained at 65 °C for 8 h to be subsequently quenched by 5x dilution in deionized water and pH was adjusted to 7.4 using 4 M HCl. Norbornene-functionalized gelatin (Gel-NOR) was synthesized to published protocol.^[7] Gelatin (10 wt.%) was dissolved in deionized water at 50 °C. 20 wt.% carbic anhydride was added, after which 10 M NaOH was added dropwise (1 mL g⁻¹ gelatin) to dissolve the carbic anhydride. The reaction was maintained at 50 °C for 24 h. Afterward, the reaction was quenched by 3x dilution in deionized water. The reaction mixture was finally centrifugated, removing the solute fraction containing unreacted carbic anhydride. After reaction, the reaction products for all macromer syntheses were individually dialyzed against deionized water (MWCO: 12–14 kDa) for 3 days at room temperature. After dialysis, the final product was collected, filtered through a 0.22 μ m sterile filter, frozen, and lyophilized. The reaction products were verified through ¹H NMR spectroscopy. The degree of modification (DoM) of PVA-MA was calculated from the proton integral of methacrylate vinyl groups relative to protons present on the PVA backbone. The DoMs of Gel-MA, Gel-AGE, and Gel-NOR were calculated from the proton integral of methacryloyl for Gel-MA and alkene groups for Gel-AGE and Gel-NOR. The proton peak from aromatic groups present on the gelatin backbone was used as a reference. Phenylalanine residues were assumed to be responsible for the aromatic group peak and contributed to 2.1% w/w, or 0.143 mmol per g gelatin, in accordance with the gelatin handbook.^[27]

Isolation of Silk Fibroin: Silk fibroin solution was isolated from Bombyx mori silkworm cocoons as previously described.^[81] Cocoons (Tajima Shoji, Japan) were cut into small pieces and boiled in 0.02 M sodium carbonate solution for 30 min in a degumming process to remove sericin from silk fibroin. The degummed silk fibroin fibers were dissolved in 9.3 M lithium bromide at 20 wt.% for 2–4 h at 60 °C until fully dissolved. The silk fibroin solution was dialyzed against deionized water (MWCO: 12–14 kDa) for 3 days at room temperature. The solution was stored at 4 °C for further use. An aliquot was taken of the silk fibroin solution to determine the concentration of the silk fibroin solution (2.56 wt.%).

Preparation and Fabrication of Casted Hydrogels: Gelatin precursor solutions consisted of gelatin (5–10 wt.%) and visible light-sensitive photo-initiators Ru (0.1–1 mM) and SPS (3–10 mM). To fabricate casted discs, precursor solutions were pipetted into a silicone mold (5.5 mm \varnothing , 1 mm height). Photo-cross-linking was then induced using an S1500

Spot UV Curing (Omnicure, MA, USA) equipped with a light filter (Rosci IR/UV filter, CT, USA) through exposure to visible light (30 mW cm⁻², 3 min, 400–450 nm).

Mass Loss and Swelling: Mass loss and mass swelling studies of casted hydrogel discs were performed after 1, 3, 7, 10, and 14 days. For each experimental group, three hydrogels were lyophilized immediately after obtaining their wet weight (m_{initial,t_0}) to determine their dry weight (m_{dry,t_0}) for calculating the macromer fraction (M%) through Equation 1. The initial wet weights (m_{swollen,t_0}) were recorded for three further hydrogels for each time point. Hydrogels were then incubated at physiological conditions (37 °C/5% CO₂) in PBS supplemented with 0.1% w/v SA, refreshing the liquid every 2 days. At each time point, swollen weight of hydrogels (m_{swollen,t_n}) were recorded and hydrogels were subsequently lyophilized to obtain the dried hydrogel weight (m_{dry,t_n}). Mass loss was defined as the relative loss of polymer in hydrogels as determined through Equation 2. Mass swelling ratio q was determined through Equation 3. The mass-loss at day 1, i.e., sol fraction, is defined as the percentage of polymers unbound in the initial polymer network after cross-linking, and was therefore be taken as a measure of cross-linking efficiency.^[30,36]

$$M\% = \frac{m_{\text{dry},t_0}}{m_{\text{initial},t_0}} \quad (1)$$

$$\text{Mass loss} = \frac{(M\% \times m_{\text{swollen},t_0}) - m_{\text{dry},t_n}}{(M\% \times m_{\text{swollen},t_0})} \times 100\% \quad (2)$$

$$\text{Swelling ratio} = m_{\text{swollen},t_n} \div m_{\text{dry},t_n} \quad (3)$$

Animal Experiments, Surgical Procedures, and Sample Processing: The animal experiments were performed with the approval of the University of Otago Animal Ethics Committee (AUP-21-24) and in accordance with the Animal Welfare Act and the ARRIVE guidelines for animal experimentation.^[82] Three 10 weeks old female Balb/c mice were housed together in IVC cages at the Christchurch Animal Research Area (CARA) of the University of Otago. Animals received standard food pellets and water ad libitum, under climate-controlled conditions (≈22 °C; 12 h light/12 h darkness). Prior to surgery, mice received a dose of Temgesic subcutaneously (0.1 mg kg⁻¹ body weight). Subcutaneous pockets were created aseptically under general anesthesia (2–3.5% isoflurane in oxygen) from 6 mm dorsal incisions and blunt dissection as previously described.^[59] In each pocket, one casted hydrogel disc (5.5 mm initial diameter, 1 mm height) composed of 10 wt.% gelatin, 0.1 mm Ru, and 3 or 10 mm SPS was implanted ($n = 3$ per group). The skin was closed with Mono Q resorbable 5-0 sutures. As pain relief treatment, mice received one additional Temgesic injection subcutaneously (0.1 mg kg⁻¹ bodyweight) 4–6 h post-surgery and a single subcutaneous injection of Carprofen (5 mg kg⁻¹ of body weight) for the following 2 days. Mice were euthanized a week after surgery with an intraperitoneal overdose of barbiturates (phenobarbital; 100 mg kg⁻¹ body weight). Implants were retrieved and fixed in 4% w/v formaldehyde. Afterward, samples were sequentially rinsed in PBS with 0.3 M glycine, PBS and embedded in a tissue freeze medium (Leica Biosystems, Germany). Cryosections of 30 μm of thickness sections were achieved using a Leica Biosystems cryostat microtome (CM1860). Sections were stained with H&E.

EBP-Based Sacrificial Printing and Construct Characterization: Extrusion of gelatin sacrificial bioinks was done using an auger-driven dispenser on a Bioscaffolder (SYS+ENG, Germany) by extruding sacrificial gelatin bioink through a 23G cylindrical needle. Bioink (22, 24, and 28.5 °C for 5, 7.5, and 10 wt.% gelatin, respectively) and collector (4 °C) temperature were separately controlled by two external Thermocubes (SSC Systems, NY, USA). Six-layered sacrificial gelatin templates (10 wt.% gelatin, 0–0.1 mm Ru, 3–10 mm SPS) were printed (23G needle, 500 mm min⁻¹, auger speed 7 rpm) in a 0–90° lattice pattern. After printing, the construct was submerged into a silicone mold (5 × 5 × 2 mm) filled with matrix hydrogel-precursor solution (10 wt.% PVA-MA with 0.1 wt.% Ig2959 or 5/5 mm/ mm TEMED/SPS, 10 wt.% Gel-MA with 0.1% Ig2959

or 5/5 mm/ mm TEMED/SPS, 10 wt.% Gel-AGE with 36 mm DTT and 0.1 wt.% Ig2959, 10 wt.% Gel-NOR with 36 mm DTT and 0.1 wt.% Ig2959, 10 wt.% Gel-AGE, 36 mm DTT, 0.5/10 mm/ mm Ru/SPS) and exposed to light to induce photo-cross-linking (30 mW cm⁻², 400–450 nm, 3 min). Constructs were incubated at physiological temperature in PBS supplemented with 0.1% w/v SA. To investigate the gelatin dissolution rate, constructs were submerged in colored PBS at various time points (4 h and 1, 3, 7, 10, 14, and 17 days), looking at infiltration of colored PBS into the lattice structure within the matrix hydrogel. In addition, cross-sections were stained with Coomassie Plus Assay Reagent for 4 h to verify the presence of gelatin internal structure or open channels (see Supporting Information).

DLP-Based Sacrificial Printing and Construct Characterization: Sacrificial gelatin templates were fabricated by exposing sacrificial gelatin bioresin (10 wt.% gelatin, 0–0.1 mm Ru, 3–10 mm SPS) to predesigned light patterns using a LumenX (Cellink, Bico Group, Sweden). To combine different sacrificial gelatin bioresins, the thermo-reversible nature of gelatin inks was exploited. Individual gelatin bioresins were sequentially cast into a silicone mold that was stuck to a glass slide. The slide was then left at room temperature to include temperature-induced physical cross-linking of the gelatin bioresin. The silicone mold was then removed to allow extrusion of a second and third ink on either side of the first ink. To obtain smooth interfaces, the glass slide was heated by the base plate of the LumenX (60 °C) for 1 min prior to exposing the bioresin to predesigned light patterns. After fabrication of the sacrificial templates, uncross-linked bioresin was washed using warm water, after which the sacrificial templates were left to cool on ice for 10 min prior to embedding the sacrificial templates in bulk hydrogel. For embedding, a thin layer (<1 mm) of bulk Gel-AGE hydrogel-precursor solution was cast into a mold and exposed to light (30 mW m⁻², 400–450 nm, 10 sec) to initiate partial cross-linking. The sacrificial template was thereafter placed on top of the bulk hydrogel. Finally, the mold was filled with bulk Gel-AGE hydrogel-precursor solution and exposed to light (30 mW cm⁻², 400–450 nm, 3 min) to achieve complete cross-linking of the Gel-AGE bulk hydrogel. Constructs were incubated at physiological temperature in PBS supplemented with 0.1% w/v SA. To investigate the dissolution of the sacrificial gelatin template, bulk hydrogels were infused with dyed PBS after 1, 4, and 11 days.

VBP-Based Sacrificial Printing and Construct Characterization: Volumetric bioprinting was achieved using a Tomolite printer (Readily3D, Switzerland) as previously described.^[56] VBP-based sacrificial printing consisted of a two-step process, namely fabrication of the bulk hydrogel and subsequent fabrication of the sacrificial template within the bulk hydrogel. First, VBP was used to fabricate bulk 10 wt.% Gel-MA hydrogels using a light dose of 210 mJ cm⁻². Post fabrication, Gel-MA hydrogels were heated to 37 °C to melt the uncross-linked bioresin. In the second step, the Gel-MA bulk hydrogel was placed inside the sacrificial gelatin bioresin (15 wt.% gelatin, 0.3 mm Ru, 50 mm SPS), after which a disc-shaped structure was printed across the circumference of the Gel-MA bulk hydrogel at a light dose of 550 mJ cm⁻². The hybrid VBP-based sacrificial printed constructs were subsequently washed and post-cured in a Ru/SPS bath. Constructs were incubated at physiological temperature in PBS supplemented with 0.1% w/v SA. To investigate the dissolution of the sacrificial gelatin template, bulk hydrogels were perfused with Alcian Blue staining solution through the inlet of the printed structure.

Fabrication and Analysis of Perfusion Microfluidics Chips: Perfusable microfluidics chips were fabricated using a Form2 SLA printer (MA, USA). A bottom hydrogel layer (10 wt.% Gel-AGE, 36 mm DTT, 0.5/10 mm/ mm Ru/SPS) is dispensed into the microfluidics chip and allowed to cool down for 10 min on the collector plate (10 °C) of the Bioscaffolder that is cooled using a Thermocube. Gelatin inks were then dispensed on top of the bottom hydrogel layer. Subsequently, a top hydrogel layer with the same composition as the bottom hydrogel layer was dispensed to fill the microfluidics chip. The total construct was finally exposed to light to induce photo-cross-linking (100 mW cm⁻², 400–450 nm, 3 min). Constructs were incubated at physiological temperature (37 °C) in PBS supplemented with 0.1% w/v SA. To

investigate gelatin dissolution, PBS supplemented with food coloring was pumped through the chips at various time points using a microfluidics pump (Harvard Apparatus, MA, USA).

Cell Isolation, Culture, and Encapsulation: Mesenchymal stromal cells (MSCs) were obtained from RoosterBio (MD, USA) and used at passage 3. MSCs were cultured (3000 cells cm⁻²) in MSC expansion media (MEM), consisting of α MEM media supplemented with 20 mM AsAp, 5 ng mL⁻¹ bFGF, 10% FBS, and 1% PS. Green fluorescent protein-transfected human umbilical vein endothelial cells (GFP-HUVECs) were purchased from Caltag Medical (UK). GFP-HUVECs were cultured (3500 cells cm⁻²) in endothelial media, consisting of vascular cell basal media supplemented with endothelial cell growth kit-VEGF according to manufacturer's instruction and PS. For cell encapsulation experiments, a bulk hydrogel consisting of 5 wt.% Gel-AGE, 18 mM DTT, 0.1/5 mm/ mm Ru/SPS was used. Sacrificial gelatin templates were incorporated within these bulk hydrogels as described earlier. Three different experiments were conducted, one aimed at osteogenesis and two different experiments aimed at neo-vascularization. **Table 2** summarizes the cell concentrations for MSCs and GFP-HUVECs within the gelatin and Gel-AGE compartments for these studies. Osteogenic constructs were cultured for 3 weeks in osteogenic differentiation media (ODM) consisting of α MEM media supplemented with 20 mM AsAp, 10 mM β -GP, 10 nM Dex, 10% FBS, and 1% PS, changing media three times per week. Experiments looking into neo-vascularization were conducted for 10 days, during which constructs were incubated in endothelial media which was changed every 2 days.

Qualitative Analysis of Mineralization: Constructs cultured under osteogenic conditions were collected after 21 days, washed in PBS, and fixed in 4% w/v formaldehyde for 1 h. To visualize mineralization in constructs cultured under osteogenic conditions, constructs were incubated in alizarin red S solution (pH 4.2) for 5 s. The constructs were then washed in deionized water multiple times before imaging the constructs using an Axioimager Z1 fluorescence microscope (Carl Zeiss, Germany).

Histological Evaluation and Quantification of Cellular Hypoxia: Hypoxia was investigated in osteogenic constructs with pimonidazole following manufacturer's protocol. Pimonidazole was reduced in hypoxic cells, resulting in the formation of stable covalent bonds between pimonidazole and proteins, peptides, and amino acids within hypoxic cells. Hypoxic cells could therefore be identified through staining for pimonidazole. Osteogenic constructs were incubated in ODM supplemented with 220 μ M pimonidazole hydrochloride for 24 h after 1, 3, and 7 days of incubation. These constructs were then fixed in 4% w/v formaldehyde overnight and washed in PBS. Constructs were infiltrated with optimal cutting temperature compound at 4 °C for 49 h and frozen at -20 °C. Samples were then cryo-sectioned into 10 μ m thick sections using a Leica Biosystems cryostat microtome (CM1860). Sections were stored at -20 °C prior to staining. For staining, sections were washed with distilled water and washing buffer (PBS supplemented with 0.2% v/v Tween20) for 2 min each. Section peroxidation was achieved through incubation of the sections in 0.3% v/v H₂O₂ for 10 min at room temperature and subsequent boiling of the sections in citrate buffer (pH 6) for 20 min at 90 °C. After rinsing sections with washing buffer, 1% PS were blocked using 5% w/v BSA

Table 2. MSC and HUVEC concentrations within the sacrificial gelatin templates and bulk Gel-AGE hydrogels.

Targeted application	Cells within sacrificial gelatin template	Cells within bulk Gel-AGE hydrogel
Bone	–	MSCs (5 million cells mL ⁻¹)
Neo-vascularization	–	MSCs, GFP-HUVECs (each 2.5 million cells mL ⁻¹)
Neo-vascularization	GFP-HUVECs (2.5 million cells mL ⁻¹)	MSCs (2.5 million cells mL ⁻¹)

for 30 min at room temperature. Sections were then in after which they were stained with primary FITC-labeled anti-pimonidazole mouse IgG1 monoclonal antibody (1:100) and secondary HRP-conjugated anti-FITC rabbit antibody (1:100) in subsequent incubation steps of 1 h separated by washing steps using washing buffer. Sections were peroxidized for 6 min in DAB and counterstained with hematoxylin. Sections were finally rinsed in distilled water and dehydrated. The dehydrated sections were mounted using DPX and imaged on an Axioimager Z1 fluorescence microscope. The number of hypoxic cells and non-hypoxic cells were manually counted in ImageJ and the percentage of hypoxic cells was then calculated using Equation 4.

$$\text{Hypoxic cells\%} = \frac{\text{Hypoxic cell count}}{\text{Total cell count}} \times 100\% \quad (4)$$

Immunohistochemical Evaluation of Capillary-Like Network Formation: Vascular constructs were collected after respectively 10 days, washed in PBS and fixed in 4% w/v formaldehyde for 1 h. Samples were washed in PBS and permeabilized with 0.25% v/v Triton X-100. Subsequently, samples were blocked with 2 wt.% BSA for 1 h and washed with PBS. Samples were incubated with primary in 1% w/v BSA overnight, after which they were stained with primary antibodies against CD31 (10 μ g mL⁻¹) and α SMA (5 μ g mL⁻¹). Samples were washed with 1% w/v BSA and subsequently incubated for 1 h with FITC- and TRITC-conjugated secondary antibodies. Then, samples were incubated with DAPI for 2 min and finally washed in PBS before imaging samples on an Axioimager Z1 fluorescence microscope. The autofluorescence of the bulk hydrogels was exploited to identify the channel positions, allowing the addition of gridlines to qualitative images to indicate the channels.

Quantification of Capillary-Like Network Formation: Capillary-like network formation was assessed through imaging a 100 μ m Z-stack of endothelial constructs after 10 days of culture using an Axioimager Z1 fluorescence microscope. For each construct, image brightness and contrast of three representative images were adjusted in ImageJ prior to quantifying average vessel length and junction density using AngioTool software.^[83] The autofluorescence of the bulk hydrogels was exploited to identify the channel positions, allowing the addition of gridlines to qualitative images to indicate the channels.

Statistical Analysis: Raw data were analyzed without pre-processing. Data were expressed as mean \pm standard deviation. All in vitro studies were repeated three times (N = 3), including triplicates (n = 3) each time, resulting in a total of nine tested samples. Results between experimental groups were analyzed by a one-way ANOVA with Tukey post hoc test. Statistical differences between different time points within one experimental group were compared through an independent sample t-test. Statistically significant differences between experimental groups of interest were depicted as *(p < 0.05), ** (p < 0.01), *** (p < 0.001), or **** (p < 0.0001), N = 3. Statistical analyses were made using GraphPad Prism software, version 9.

Supporting Information

Supporting Information is available from the Wiley Online Library or from the author.

Acknowledgements

K.L. would like to acknowledge funding support from the Health Research Council of New Zealand (Sir Charles Hercus Health Research Fellowship 19/135, Project Grant 20/508, Emerging Researcher First Grant 15/483), and Royal Society Te Apārangi (Marsden Fast Start Grant MFP-U001826). G.L. was supported by the Emerging Researcher First Grant 19/679, Explorer 21/802, and University of Otago Health Science Postdoctoral Fellowship. T.W., K.L., G.L., and B.S. acknowledge funding support from the Medical Technologies Centre of Research

Excellence (MedTech CoRE). J.R.-K. was partially supported by the Heart Foundation of Australia Future Leader Fellowship (101896). R.L. acknowledges funding from the European Research Council (ERC) under the European Union's Horizon 2020 research and innovation programme (grant agreement No. 949806, VOLUME-BIO) and from the European Union's Horizon 2020 research and innovation programme under grant agreement No 964497 (ENLIGHT). The authors would like to thank Nuria Gines Rodriguez and Gabriel Größbacher for their help with the volumetric printing experiments.

Open access publishing facilitated by University of Otago, as part of the Wiley - University of Otago agreement via the Council of Australian University Librarians.

Conflict of Interest

The authors declare no conflict of interest.

Data Availability Statement

The data that support the findings in this paper are available from the corresponding author upon reasonable request.

Keywords

biofabrication, bioprinting, hydrogels, neo-vascularization, osteogenesis, sacrificial printing

Received: October 16, 2022

Revised: December 19, 2022

Published online: January 12, 2023

- [1] W. He, M. Reaume, M. Hennenfent, B. P. Lee, R. Rajachar, *Biomater. Sci.* **2020**, *8*, 3248.
- [2] J. A. Burdick, W. L. Murphy, *Nat. Commun.* **2012**, *3*, 1269.
- [3] F. M. R. Witjas, B. M. van den Berg, C. W. van den Berg, M. A. Engelse, T. J. Rabelink, *Stem Cells Transl. Med.* **2019**, *8*, 375.
- [4] H. Shi, C. Wang, Z. Ma, *APL Bioeng.* **2021**, *5*, 011506.
- [5] J. Rouwkema, A. Khademhosseini, *Trends Biotechnol.* **2016**, *34*, 733.
- [6] J. S. Miller, K. R. Stevens, M. T. Yang, B. M. Baker, D. H. T. Nguyen, D. M. Cohen, E. Toro, A. A. Chen, P. A. Galie, X. Yu, R. Chaturvedi, S. N. Bhatia, C. S. Chen, *Nat. Mater.* **2012**, *11*, 768.
- [7] B. G. Soliman, G. S. Major, P. Atienza-Roca, C. A. Murphy, A. Longoni, C. R. Alcalá-Orozco, J. Rnjak-Kovacina, D. Gawlitta, T. B. F. Woodfield, K. S. Lim, *Adv. Healthcare Mater.* **2022**, *11*, 2101873.
- [8] J. H. Jeong, V. Chan, C. Cha, P. Zorlutuna, C. Dyck, K. J. Hsia, R. Bashir, H. Kong, *Adv. Mater.* **2012**, *24*, 58.
- [9] C. Feng, W. Zhang, C. Deng, G. Li, J. Chang, Z. Zhang, X. Jiang, C. Wu, C. Feng, C. Deng, J. Chang, C. Wu, W. Zhang, G. Li, X. Jiang, Z. Zhang, *Adv. Sci.* **2017**, *4*, 1700401.
- [10] D. Loessner, C. Meinert, E. Kaemmerer, L. C. Martine, K. Yue, P. A. Levett, T. J. Klein, F. P. W. Melchels, A. Khademhosseini, D. W. Huttmacher, *Nat. Protoc.* **2016**, *11*, 727.
- [11] S. Bertlein, G. Brown, K. S. Lim, T. Jungst, T. Boeck, T. Blunk, J. Tessmar, G. J. Hooper, T. B. F. Woodfield, J. Groll, *Adv. Mater.* **2017**, *29*, 1703404.
- [12] L. Ouyang, J. P. K. Armstrong, Q. Chen, Y. Lin, M. M. Stevens, *Adv. Funct. Mater.* **2020**, *30*, 1908349.
- [13] J. W. Andrejcsk, C. C. W. Hughes, *Curr. Opin. Biomed. Eng.* **2018**, *5*, 74.
- [14] B. J. Klotz, K. S. Lim, Y. X. Chang, B. G. Soliman, I. Pennings, F. P. W. Melchels, T. B. F. Woodfield, A. J. W. P. Rosenberg, J. Malda, D. Gawlitta, *Eur. Cells Mater.* **2018**, *35*, 335.
- [15] D. B. Kolesky, R. L. Truby, A. S. Gladman, T. A. Busbee, K. A. Homan, J. A. Lewis, *Adv. Mater.* **2014**, *26*, 3124.
- [16] D. B. Kolesky, K. A. Homan, M. A. Skylar-Scott, J. A. Lewis, *Proc. Natl. Acad. Sci. USA* **2016**, *113*, 3179.
- [17] R. Levato, K. S. Lim, W. Li, A. U. Asua, L. B. Peña, M. Wang, M. Falandt, P. N. Bernal, D. Gawlitta, Y. S. Zhang, T. B. F. Woodfield, J. Malda, *Materials Today Bio* **2021**, *12*, 100162.
- [18] P. N. Bernal, M. Bouwmeester, J. Madrid-wolff, M. Falandt, S. Florczak, N. G. Rodriguez, Y. Li, G. Größbacher, R. Samsom, M. Van Wolferen, L. J. W. Van Der Laan, P. Delrot, D. Loterie, J. Malda, C. Moser, B. Spee, R. Levato, *Adv. Mater.* **2022**, *34*, 2110054.
- [19] B. Berman, *Business Horizons* **2012**, *55*, 155.
- [20] J. Groll, T. Boland, T. Blunk, J. A. Burdick, P. D. Dalton, B. Derby, G. Forgacs, Q. Li, V. A. Mironov, L. Moroni, N. Makoto, W. Shu, S. Takeuchi, G. Vozzi, T. B. F. Woodfield, T. Xu, J. J. Yoo, J. Malda, *Biofabrication* **2016**, *8*, 013001.
- [21] B. Byambaa, N. Annabi, K. Yue, G. Trujillo-de Santiago, M. M. Alvarez, W. Jia, M. Kazemzadeh-Narbat, S. R. Shin, A. Tamayol, A. Khademhosseini, *Adv. Healthcare Mater.* **2017**, *6*, 1700015.
- [22] M. Ryma, H. Genç, A. Nadernezhad, I. Paulus, D. Schneidereit, O. Friedrich, K. Andelovic, S. Lyer, C. Alexiou, I. Cicha, J. Groll, *Adv. Mater.* **2022**, *34*, 2200653.
- [23] W. Liu, M. A. Heinrich, Y. Zhou, A. Akpek, N. Hu, X. Liu, X. Guan, Z. Zhong, X. Jin, A. Khademhosseini, Y. S. Zhang, *Adv. Healthcare Mater.* **2017**, *6*, 1601451.
- [24] C. M. Elvin, T. Vuocolo, A. G. Brownlee, L. Sando, M. G. Huson, N. E. Liyou, P. R. Stockwell, R. E. Lyons, M. Kim, G. A. Edwards, G. Johnson, G. A. McFarland, J. A. M. Ramshaw, J. A. Werkmeister, *Biomaterials* **2010**, *31*, 8323.
- [25] K. S. Lim, Y. Ramaswamy, J. J. Roberts, M.-H. Alves, L. A. Poole-Warren, P. J. Martens, *Macromol. Biosci.* **2015**, *15*, 1423.
- [26] K. S. Lim, J. J. Roberts, M.-H. Alves, L. A. Poole-Warren, P. J. Martens, *J. Appl. Polym. Sci.* **2015**, *132*, 42142.
- [27] P. Atienza-Roca, D. C. Kieser, X. Cui, B. Bathish, Y. Ramaswamy, G. J. Hooper, A. N. Clarkson, J. Rnjak-Kovacina, P. J. Martens, L. M. Wise, T. B. F. Woodfield, K. S. Lim, *Biomater. Sci.* **2020**, *8*, 5005.
- [28] B. G. Soliman, G. C. J. Lindberg, T. Jungst, G. J. Hooper, J. Groll, T. B. F. Woodfield, K. S. Lim, *Adv. Healthcare Mater.* **2020**, *9*, 1901544.
- [29] S. I. Belli, M. G. Wallach, C. Luxford, M. J. Davies, N. C. Smith, *Eukaryotic Cell* **2003**, *2*, 456.
- [30] S. Mukherjee, E. A. Kapp, A. Lothian, A. M. Roberts, Y. V. Vasil'Ev, B. A. Boughton, K. J. Barnham, W. M. Kok, C. A. Hutton, C. L. Masters, A. I. Bush, J. S. Beckman, S. G. Dey, B. R. Roberts, *Anal. Chem.* **2017**, *89*, 6136.
- [31] K. S. Lim, B. S. Schon, N. V. Mekhileri, G. C. J. Brown, C. M. Chia, S. Prabakar, G. J. Hooper, T. B. F. Woodfield, *ACS Biomaterials Science and Engineering* **2016**, *2*, 1752.
- [32] K. S. Lim, B. J. Klotz, G. C. J. Lindberg, F. P. W. Melchels, G. J. Hooper, J. Malda, D. Gawlitta, T. B. F. Woodfield, K. S. Lim, G. C. J. Lindberg, G. J. Hooper, T. B. F. Woodfield, B. J. Klotz, D. Gawlitta, J. Malda, F. P. W. Melchels, G. C. J. Lindberg, F. P. W. Melchels, G. J. Hooper, J. Malda, D. Gawlitta, T. B. F. Woodfield, *Macromol. Biosci.* **2019**, *19*, 1900098.
- [33] D. A. Fancy, T. Kodadek, *Proc. Natl. Acad. Sci. USA* **1999**, *96*, 6020.
- [34] D. A. Fancy, C. Denison, K. Kim, Y. Xie, T. Holdeman, F. Amini, T. Kodadek, *Chem. Biol.* **2000**, *7*, 697.
- [35] A. Radzicka, R. Wolfenden, *J. Am. Chem. Soc.* **1996**, *118*, 6105.
- [36] C. A. Lewis, R. Wolfenden, *J. Am. Chem. Soc.* **2014**, *136*, 130.
- [37] D. M. Kirchmayer, C. A. Watson, M. Ranson, M. In Het Panhuis, *RSC Adv.* **2013**, *3*, 1073.
- [38] S. Lyu, D. Untereker, *Int. J. Mol. Sci.* **2009**, *10*, 4033.

- [39] K. S. Lim, M. H. Alves, L. A. Poole-Warren, P. J. Martens, *Biomaterials* **2013**, *34*, 7097.
- [40] M. M. Welz, C. M. Ofner, *J. Pharm. Sci.* **1992**, *81*, 85.
- [41] T. B. F. Woodfield, C. A. Van Blitterswijk, J. De Wijn, T. J. Sims, A. P. Hollander, J. Riesle, *Tissue Eng.* **2005**, *11*, 1297.
- [42] V. H. M. Mouser, F. P. W. Melchels, J. Visser, W. J. A. Dhert, D. Gawlitta, J. Malda, *Biofabrication* **2016**, *8*, 035003.
- [43] L. Rebers, R. Reichsöllner, S. Regett, G. E. M. Tovar, K. Borchers, S. Baudis, A. Southan, *Sci. Rep.* **2021**, *11*, 3256.
- [44] J. Van Hoorick, L. Tytgat, A. Dobos, H. Ottevaere, J. Van Erps, H. Thienpont, A. Ovsianikov, P. Dubruel, S. Van Vlierberghe, *Acta Biomater.* **2019**, *97*, 46.
- [45] M. Tavafoghi, M. A. Darabi, M. Mahmoodi, R. Tutar, C. Xu, A. Mirjafari, F. Billi, W. Swieszkowski, F. Nasrollahi, S. Ahadian, V. Hosseini, A. Khademhosseini, N. Ashammakhi, *Biofabrication* **2021**, *13*, 042002.
- [46] R. Censi, T. Vermonden, H. Deschout, K. Braeckmans, P. Di Martino, S. C. De Smedt, C. F. Van Nostrum, W. E. Hennink, *Biomacromolecules* **2010**, *11*, 2143.
- [47] C. C. Lin, A. T. Metters, *Adv. Drug Delivery Rev.* **2006**, *58*, 1379.
- [48] R. Murphy, D. P. Walsh, C. A. Hamilton, S. A. Cryan, M. In Het Panhuis, A. Heise, *Biomacromolecules* **2018**, *19*, 2691.
- [49] B. J. Carberry, J. E. Hergert, F. M. Yavitt, J. J. Hernandez, K. F. Speckl, C. N. Bowman, R. R. McLeod, K. S. Anseth, *Biofabrication* **2021**, *13*, 044104.
- [50] N. Brandenberg, M. P. Lutolf, *Adv. Mater.* **2016**, *28*, 7450.
- [51] J. Hu, Y. Hou, H. Park, B. Choi, S. Hou, A. Chung, M. Lee, *Acta Biomater.* **2012**, *8*, 1730.
- [52] G. C. J. Lindberg, K. S. Lim, B. G. Soliman, A. Nguyen, G. J. Hooper, R. J. Narayan, T. B. F. Woodfield, *Appl. Phys. Rev.* **2021**, *8*, 011301.
- [53] K. S. Lim, J. H. Galarraga, X. Cui, G. C. J. Lindberg, J. A. Burdick, T. B. F. Woodfield, *Chem. Rev.* **2020**, *120*, 10662.
- [54] X. Zhou, Z. Li, *Adv. Healthcare Mater.* **2018**, *7*, 1800020.
- [55] L. Moroni, T. Boland, J. A. Burdick, C. De Maria, B. Derby, G. Forgacs, J. Groll, Q. Li, J. Malda, V. A. Mironov, C. Mota, M. Nakamura, W. Shu, S. Takeuchi, T. B. F. Woodfield, T. Xu, J. J. Yoo, G. Vozzi, *Trends Biotechnol.* **2018**, *36*, 384.
- [56] P. Nuñez Bernal, P. Delrot, D. Loterie, Y. Li, J. Malda, C. Moser, R. Levato, P. N. Bernal, Y. Li, J. Malda, R. Levato, P. Delrot, D. Loterie, C. Moser, Y. Li, J. Malda, C. Moser, R. Levato, *Adv. Mater.* **2019**, *31*, 1904209.
- [57] F. L. C. Morgan, L. Moroni, M. B. Baker, *Adv. Healthcare Mater.* **2020**, *9*, 1901798.
- [58] X. Ma, X. Qu, W. Zhu, Y.-S. S. Li, S. Yuan, H. Zhang, J. Liu, P. Wang, C. S. E. Lai, F. Zanella, G.-S. S. Feng, F. Sheikh, S. Chien, S. Chen, **2016**, *113*, 2206.
- [59] K. S. Lim, R. Levato, P. F. Costa, M. D. Castilho, C. R. Alcalá-Orozco, K. M. A. Van Dorenmalen, F. P. W. W. Melchels, D. Gawlitta, G. J. Hooper, J. Malda, T. B. F. F. Woodfield, K. M. A. van Dorenmalen, F. P. W. W. Melchels, D. Gawlitta, G. J. Hooper, J. Malda, T. B. F. F. Woodfield, *Biofabrication* **2018**, *10*, 034101.
- [60] W. Li, M. Wang, L. S. Mille, J. A. R. Lara, V. Huerta, T. U. Velázquez, F. Cheng, H. Li, J. Gong, T. Ching, C. A. Murphy, A. Lesha, S. Hassan, T. B. F. Woodfield, K. S. Lim, Y. S. Zhang, *Adv. Mater.* **2021**, *33*, 2102153.
- [61] B. E. Kelly, I. Bhattacharya, H. Heidari, M. Shusteff, C. M. Spadaccini, H. K. Taylor, **2019**, *363*, 1075.
- [62] A. R. Armiento, L. P. Hatt, G. Sanchez Rosenberg, K. Thompson, M. J. Stoddart, *Adv. Funct. Mater.* **2020**, *30*, 1909874.
- [63] M. Radisic, J. Malda, E. Epping, W. Geng, R. Langer, G. Vunjak-Novakovic, *Biotechnol. Bioeng.* **2006**, *93*, 332.
- [64] K. S. Lim, M. Baptista, S. Moon, T. B. F. Woodfield, J. Rnjak-Kovacina, *Trends Biotechnol.* **2019**, *37*, 1189.
- [65] S. M. Vickers, L. L. Johnson, L. Q. Zou, I. V. Yannas, L. J. Gibson, M. Spector, *Tissue Eng.* **2004**, *10*, 1214.
- [66] X. Sun, Y. Wei, *Cytotherapy* **2009**, *11*, 261.
- [67] D. Yang, M. Yang, C. Tsai, T. Huang, Y. Chen, *PLoS One* **2011**, *6*, e23965.
- [68] D. Li, Z. Yang, X. Zhao, Y. Luo, Y. Ou, P. Kang, M. Tian, *J. Mater. Chem. B* **2021**, *9*, 479.
- [69] H. A. O. Ding, S. Chen, J. Yin, X. Xie, Z. H. Zhu, *Mol. Med. Rep.* **2014**, *2184*.
- [70] X. Yu, Q. Wan, X. Ye, Y. Cheng, J. L. Pathak, Z. Li, *Cell. Mol. Biol. Lett.* **2019**, *24*, 64.
- [71] M. Wagegg, T. Gaber, F. L. Lohanatha, M. Hahne, C. Strehl, P. Hoff, A. Ode, M. Fangradt, C. L. Tran, K. Scho, C. Perka, G. N. Duda, F. Buttgerit, *PLoS One* **2012**, *7*, e46483.
- [72] S. A. Eming, P. Martin, M. Tomic-Canic, *Sci. Transl. Med.* **2014**, *6*, 265.
- [73] A. Ueda, R. Sudo, M. Ikeda, K. I. Kokubo, S. Kudo, H. Kobayashi, K. Tanishita, *J. Biomech. Sci. Eng.* **2008**, *3*, 299.
- [74] C. K. Griffith, S. C. George, *Tissue Eng., Part A* **2009**, *15*, 2423.
- [75] G.-L. Ying, Y. S. Zhang, *Adv. Mater.* **2018**, *30*, 1805460.
- [76] S. Yi, Q. Liu, Z. Luo, J. J. He, H.-L. Ma, W. Li, D. Wang, C. Zhou, C. E. Garciamendez, L. Hou, J. Zhang, Y. S. Zhang, *Small* **2022**, *18*, 2106357.
- [77] R. Levato, T. Jungst, R. G. Scheuring, T. Blunk, J. Groll, J. Malda, *Adv. Mater.* **2020**, *32*, 1906423.
- [78] P. Au, J. Tam, D. Fukumura, R. K. Jain, *Blood* **2008**, *111*, 4551.
- [79] N. Annabi, J. W. Nichol, X. Zhong, C. Ji, S. Koshy, A. Khademhosseini, F. Dehghani, *Tissue Eng. – Part B: Rev.* **2010**, *16*, 371.
- [80] M. J. Gupte, W. B. Swanson, J. Hu, X. Jin, H. Ma, Z. Zhang, Z. Liu, K. Feng, G. Feng, G. Xiao, N. Hatch, Y. Mishina, P. X. Ma, *Acta Biomater.* **2018**, *82*, 1.
- [81] X. Cui, B. G. Soliman, C. R. Alcalá-Orozco, J. Li, M. A. M. Vis, M. Santos, S. G. Wise, R. Levato, J. Malda, T. B. F. Woodfield, J. Rnjak-kovacina, K. S. Lim, *Adv. Healthcare Mater.* **2020**, *9*, 1901667.
- [82] N. Percie du Sert, V. Hurst, A. Ahluwalia, S. Alam, M. T. Avey, M. Baker, W. J. Browne, A. Clark, I. C. Cuthill, U. Dirnagl, M. Emerson, P. Garner, S. T. Holgate, D. W. Howells, N. A. Karp, S. E. Lazic, K. Lidster, C. J. MacCallum, M. Macleod, E. J. Pearl, O. H. Petersen, F. Rawle, P. Reynolds, K. Rooney, E. S. Sena, S. D. Silberberg, T. Steckler, H. Würbel, *J. Cereb. Blood Flow Metab.* **2020**, *40*, 1769.
- [83] E. Zudaire, L. Gambardella, C. Kurcz, S. Vermeren, *PLoS One* **2011**, *6*, e27385.